

Graphene based inks for printed electronics

by

Wenjun Xiang

B.S., Qingdao University, 2017

A THESIS

submitted in partial fulfillment of the requirements for the degree

MASTER OF SCIENCE

Department of Industrial and Manufacturing Systems Engineering  
Carl R. Ice College of Engineering

KANSAS STATE UNIVERSITY  
Manhattan, Kansas

2021

Approved by:

Major Professor  
Suprem R. Das

# Copyright

© Wenjun Xiang 2021.

## **Abstract**

The outstanding properties of graphene make it attractive to be used as a conductive filler in inks that play an important role in printed electronics. In this thesis, liquid-phase exfoliation of pristine graphite, with the addition of ethyl cellulose stabilizer in ethanol, is employed to prepare high concentration graphene dispersions. Subsequently, the exfoliated graphene nano-flakes were collected and redispersed in cyclohexanone/terpineol solvent to form inks which were successfully inkjet printed on flexible polyimide substrates. The ideal synthesis conditions for the yielding of high concentration graphene inks including the concentration of surfactants (C), sonication time (t) and sonication energy (E) were examined. Ultraviolet–visible spectroscopy (UV-Vis) and electrical resistance were performed on the ink to show optimized results. Graphene-graphene aerosol gel (Graphene-GAGs) and graphene-multi-walled carbon nanotubes (Graphene-MWCNTs) hybrid inks, based on the optimized ink, were successfully synthesized for inkjet printing. Compared with pure graphene devices, the graphene-graphene aerosol gel (Graphene-GAGs) and graphene-multi-walled carbon nanotubes (Graphene-MWCNTs) electrodes exhibited superior electrochemical performance as demonstrated by the cyclic voltammetry test with hexaammineruthenium(III) chloride, indicating their promising application in electrochemical sensors. While the use of synthesized graphene as a matrix compared well with commercial graphene ink, potential for further improvements remains open in this research field.

# Table of Contents

|   |     |
|---|-----|
| List of Figures .....   | v   |
| List of Tables .....  | vii |
| Chapter 1 - Introduction .....  | 1   |
| 1.1 Introduction of graphene .....                                      | 1   |
| 1.1.1 Structure and properties of graphene .....                        | 1   |
| 1.1.2 Synthesis of graphene .....                                       | 6   |
| 1.2 Graphene-based conductive inks .....                                | 12  |
| 1.2.1 Motivation.....   | 12  |
| 1.2.2 Synthesis of graphene conductive inks .....                       | 15  |
| 1.3 Recent progress of graphene-based conductive inks .....             | 23  |
| 1.3.1 Classification of graphene-based conductive inks .....            | 23  |
| 1.3.2 Devices and applications.....                                     | 28  |
| 1.4 Outline of the thesis .....   | 33  |
| Chapter 2 - Synthesis and optimization of graphene conductive inks..... | 35  |
| 2.1 Formulation of graphene inks .....                                  | 35  |
| 2.2 Optimization of graphene inks.....                                  | 37  |
| 2.2.1 Ultraviolet–visible spectroscopy (UV-Vis) .....                   | 38  |
| 2.2.2 Electrical resistance measurements.....                           | 41  |
| 2.2.3 Dynamic light scattering (DLS).....                               | 44  |
| Chapter 3 - Electrochemical properties .....                            | 46  |
| 3.1 Graphene and hybrid graphene conductive inks.....                   | 46  |
| 3.2 Fabrication of electrodes .....                                     | 48  |
| 3.3 Cyclic voltammetry (CV) .....                                       | 49  |
| Chapter 4 - Summary and outlook.....                                    | 55  |
| 4.1 Summary of thesis research .....                                    | 55  |
| 4.2 Outlook .....   | 57  |
| References.....   | 59  |

## List of Figures

|   |    |
|---|----|
| Figure 1.1. (a) Sigma ( $\sigma$ ) bond and pi ( $\pi$ ) bond formed by $sp^2$ hybridization. (b) The crystal lattice of graphene, where A and B are carbon atoms belonging to different sub-lattices, $a_1$ and $a_2$ are unit-cell vectors. (reproduced with permission from Ref [6]) .....       | 2  |
| Figure 1.2. (a, b) Electronic band structures and Raman scattering processes of monolayer graphene and AB-stacked bilayer graphene, respectively. (c, d) Electronic band structures for AB-stacked trilayer and four-layer graphene, respectively. (reproduced with permission from Ref [13]) ..... | 4  |
| Figure 1.3. Raman spectra of graphene-based materials, including graphite, 1LG, 3LG, disordered graphene, graphene oxide and nanographene. (reproduced with permission from Ref [20]) .....   | 6  |
| Figure 1.4. TEM image of micromechanical cleavage graphene film after electron-beam lithography and etching step. (reproduced with permission from Ref [23]) .....  | 7  |
| Figure 1.5. Unzipping multiwalled carbon nanotubes by plasma etching of nanotubes partly embedded in a polymer film. (reproduced with permission from Ref [50]) .....   | 12 |
| Figure 1.6. Applications of graphene and graphene-based materials. (reproduced with permission from Ref [64]) .....   | 15 |
| Figure 1.7. Graphene produce methods with evaluation in terms of quality (G), yield (Y), cost aspect (C; a low value corresponds to high cost of production), purity (P) and scalability (S). (reproduced with permission from Ref [65]) .....  | 17 |
| Figure 1.8. Liquid-phase exfoliation process of graphite in the absence and presence of surfactants. (reproduced with by permission from Ref [72]) .....  | 19 |
| Figure 1.9. Schematic illustration of solvothermal-assisted exfoliation and dispersion of graphene sheets in ACN. (reproduced with permission from Ref [79]) .....  | 23 |
| Figure 1.10. Schematic illustrates the preparation process of pristine graphene ink and its printed electrodes. (reproduced with permission from Ref [87]) .....  | 26 |
| Figure 1.11. Photographs of a $12S \times 12P$ MSC array on silicon wafer (a) and Kapton (b). (C) CV profiles of the $12S \times 12P$ MSC array at different scan rates with a voltage window of 12 V. (reproduced with permission from Ref [98]) .....   | 31 |

|   |    |
|---|----|
| Figure 1.12. Schematic representation of the proposed humidity sensor. (reproduced with permission from Ref [100]) .....  | 32 |
| Figure 2.1. UV-Vis spectrum of graphene inks at different concentrations of ethyl cellulose with 2h sonication time and 100% sonication energy.....   | 39 |
| Figure 2.2. (a) the original UV-Vis absorption spectra and (b) the scatter plot of graphene ink absorbance of 12 batches of graphene inks with three variables- the concentration of ethyl cellulose (5 mg ml <sup>-1</sup> and 10 mg ml <sup>-1</sup> ), sonication energy (50%E, and 100%E) and sonication time (2h, 4h, and 6h). .....   | 41 |
| Figure 2.3. (a) Graphene inks with different EC concentration (mg ml <sup>-1</sup> ), sonication energy (E) and sonication time (hr), (C, E, t): (5, 50%, 2), (5, 50%, 4), (5, 50%, 6), (5, 100%, 2), (5, 100%, 4), (5, 100%, 6), (10, 50%, 2), (10, 50%, 4), (10, 50%, 6), (10, 100%, 2), (10, 100%, 4), (10, 100%, 6), (15, 100%, 2), and (20, 100%, 2). (b) represented inkjet-printed graphene patterns with 5 mm x 5 mm area and two printing passes printed on polyimide substrates, with ink (5, 100%, 6). ..... | 43 |
| Figure 3.1. Schematic of graphene composite ink fabrication and inkjet printing process.....  | 49 |
| Figure 3.2. Cyclic voltammograms of graphene (black), graphene-GAGs (blue) and graphene-MWCNTs (red) sensors based on (a) the synthesized graphene ink and (b) a commercial graphene ink in 5.0mM [Ru(NH <sub>3</sub> ) <sub>6</sub> ] <sup>2+/3+</sup> containing 0.1M KCl at the scan rate of 100 mV s <sup>-1</sup> . .....  | 50 |
| Figure 3.3. Cyclic voltammograms of synthesized graphene ink-based graphene-GAGs electrode (a) and graphene-MWCNTs electrode (c) in 5.0mM [Ru(NH <sub>3</sub> ) <sub>6</sub> ] <sup>2+/3+</sup> in 0.1M KCl with scan rates: 5, 10, 25, 50 and 100 mV s <sup>-1</sup> . The dependence of the peak current at graphene-GAGs electrode (b) and graphene-MWCNTs electrode (d) on the square root of scan rates. ....  | 52 |
| Figure 3.4. Cyclic voltammograms of commercial graphene ink-based graphene-GAGs electrode (a) and graphene-MWCNTs electrode (c) in 5.0mM [Ru(NH <sub>3</sub> ) <sub>6</sub> ] <sup>2+/3+</sup> in 0.1M KCl with scan rates: 5, 10, 25, 50 and 100 mV s <sup>-1</sup> . The dependence of the peak current at graphene-GAGs electrode (b) and graphene-MWCNTs electrode (d) on the square root of scan rates. ....   | 54 |

## List of Tables

|  |    |
|--|----|
| Table 1.1. Surface tension, boiling point and chemical structure of some common organic solvents. .... | 20 |
| Table 1.2. Chemical structure of some common surfactants. ....   | 22 |
| Table 2.1. Resistance of printed graphene patterns. ....   | 43 |
| Table 2.2. Particle size of graphene/EC particles in inks. ....  | 44 |

# Chapter 1 - Introduction

## 1.1 Introduction to graphene

### 1.1.1 Structure and properties of graphene

Graphene has been extensively studied and received lots of scientific and public attention in the past few decades due to the large surface areas, high thermal conductivity, high electron mobility, strong chemical durability and excellent mechanical stability, even though it was only isolated for the first time in 2004 [1]. In fact, the first study on graphene or graphite can be dated to as early as 1947 when Wallace investigated the electronic energy bands in crystalline graphite [2]. In 1997, to evaluate the effect of graphite crystals thickness on electrical properties, Japanese scientists successfully cleaved kish graphite and reduced the thickness of the graphite films to 30 nm [3]. In 2004, Novoselov and Geim published groundbreaking work, presenting a robust and reliable approach, the mechanical exfoliation method, also called the scotch tape method, for producing monolayer graphene by repeatedly peeling highly oriented pyrolytic graphite (HOPG) [1], for which they later shared the Nobel Prize in 2010.

Graphene theoretically refers to a monolayer of graphite, with  $sp^2$  hybridized carbon atoms arranged in a hexagonal lattice and partially filled  $\pi$ -orbitals above and below the plane of the sheet [4]. The nucleus of carbon is surrounded by six electrons, four of which are valence electrons. A honeycomb network with planar structure is formed when carbon atoms share  $sp^2$  electrons with their three neighboring carbon atoms. The resulting covalent  $\sigma$  bond has a short interatomic length of  $\sim 1.42 \text{ \AA}$ , making it even stronger than the  $sp^3$  hybridized carbon-carbon bonds in diamonds, resulting in the remarkable mechanical properties of monolayer graphene [5]. The fourth bond is a  $\pi$ -bond, which is oriented in the  $z$ -direction. The  $\pi$  orbital can be viewed as a pair of symmetric lobes oriented along the  $z$ -axis and centered about the nucleus [2]. The  $\pi$ -bonds provide a weak

van der Waals interaction between adjacent graphene layers in bilayer and multi-layer graphene. The unit cell of a graphene crystal, contains two carbon atoms, and the unit-cell vectors  $a_1$  and  $a_2$  have the same lattice constant of 2.46 Å.

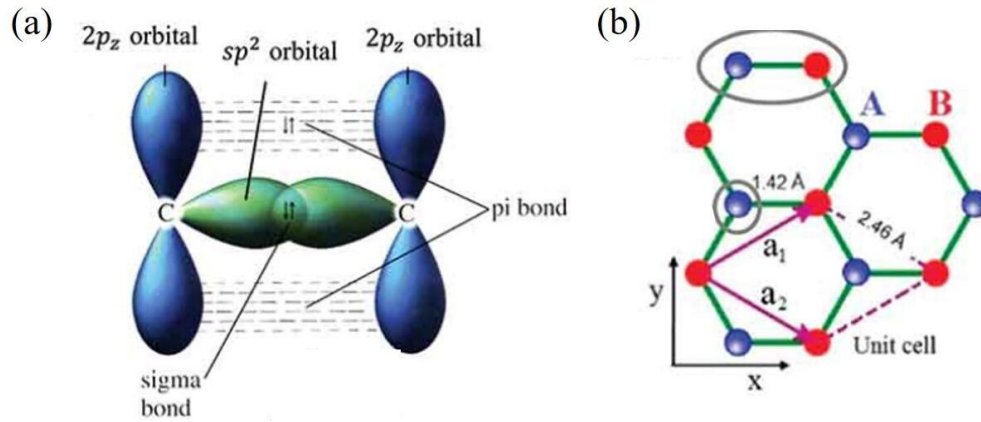


Figure 1.1. (a) Sigma ( $\sigma$ ) bond and pi ( $\pi$ ) bond formed by  $sp^2$  hybridization. (b) The crystal lattice of graphene, where A and B are carbon atoms belonging to different sub-lattices,  $a_1$  and  $a_2$  are unit-cell vectors. (reproduced with permission from Ref [6])

Except the unique structure of graphene, the electronic band which reveals the relationship between the energy and momentum of electrons within graphene has also been widely studied. Since graphene constrains the motion of electrons to two dimensions, the momentum space is also constrained to two dimensions. Even though graphene theoretically refers to monolayer graphene, the term ‘graphene’ is commonly prefixed by ‘monolayer’, ‘bilayer’ or ‘few-layer’. This categorization has been made as the electronic properties of bi- and few-layer graphene (number of layers from 3 to 10) are distinct from graphite. Bilayer graphene exhibits many of the properties featured by single layer graphene such as semi-metallicity and notable transport properties [7]. The electronic structure of few-layer graphene is more complex and 10 layers-graphene has been

shown to approach the 3D limit of graphite [8]. In monolayer graphene, the highest occupied molecular orbital (HOMO) touches the lowest unoccupied molecular orbital (LUMO) at a single Dirac point as shown in Figure 1.2(a). Due to the single  $\pi$  electron valence band and  $\pi^*$  conduction band, only one Raman scattering cycle is excited near the Dirac point. The presence of massive chiral quasiparticles at low energy leads to linear electron dispersion near the Dirac point [9]. In bilayer graphene, the interaction of the two graphene planes causes the  $\pi$  and  $\pi^*$  electron bands to divide into four parabolic band structures denoted as  $\pi_1$ ,  $\pi_2$ ,  $\pi_1^*$ , and  $\pi_2^*$ . Only two pairs of electrons can be excited by incident laser ( $\pi_1 \leftrightarrow \pi_1^*$  and  $\pi_2 \leftrightarrow \pi_2^*$ ), among the four bands according to space–group theory [10]. Figure 1.2(b) shows the four parabolic bands in (AB-stacked) bilayer graphene. The band structure of (ABA-stacked) trilayer graphene seems to be a combination of monolayer and (AB-stacked) bilayer, Figure 1.2(c). The behavior of trilayer graphene significantly differs from monolayer and bilayer graphene, which is originated from the presence of a finite overlap between valence and conduction band [11]. In few-layer graphene (number of layers from 3 to 10), the electronic bands split into more complex and dispersive configurations (Figure 1.2(d)) and therefore excited electron–hole pairs are involved in more scattering events [12]. For few-layer graphene, increased number of layers inhibits carrier mobility, which reduces conductivity.

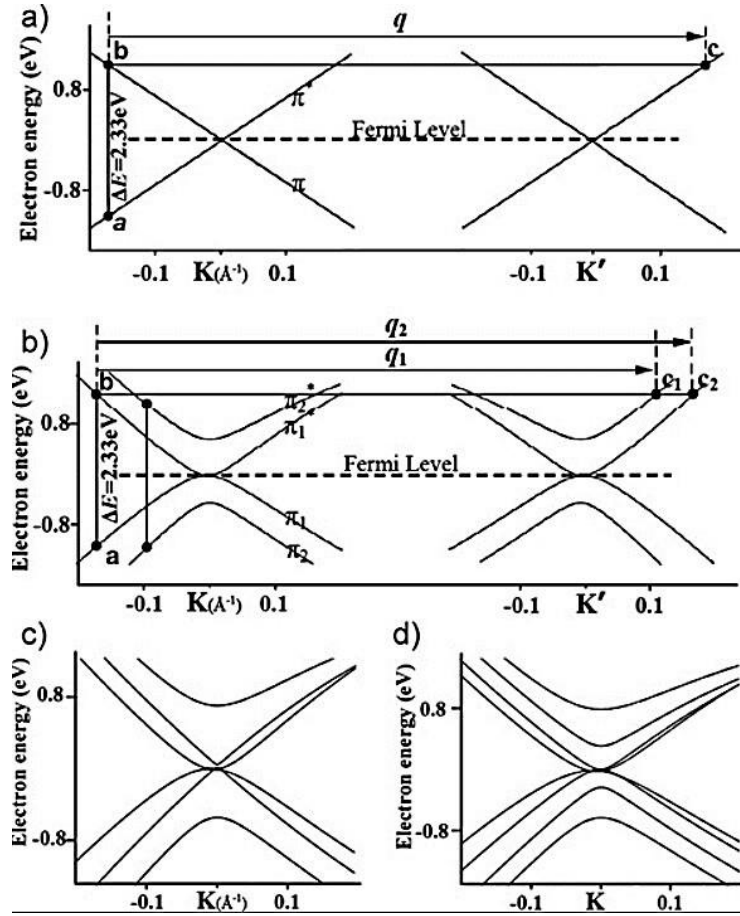


Figure 1.2. (a, b) Electronic band structures and Raman scattering processes of monolayer graphene and AB-stacked bilayer graphene, respectively. (c, d) Electronic band structures for AB-stacked trilayer and four-layer graphene, respectively. (reproduced with permission from Ref [13])

To identify different thicknesses of graphene (monolayer, bilayer, multilayer), optical microscopy (contrast), electron microscopy, atomic force microscopy, and Raman spectroscopy are being extensively used. Under optical microscopy, the monolayer graphene becomes visible on SiO<sub>2</sub> with the proper thickness of SiO<sub>2</sub>, wavelength of light, and angle of illumination [14]. This characterization is widely used for the quick identification of single- or few-layer graphene sheets, especially those obtained by mechanical exfoliation. Transmission electron microscopy has been used to image graphene sheets with the support of a microfabricated scaffold [15].

Raman spectroscopy is one of the most accurate and rapid method to determine the number of graphene layers and stacking order as well as density of defects and impurities. The major features of the Raman spectra of graphene and other graphitic materials are the disorder-induced D band at  $\sim 1350\text{ cm}^{-1}$ , the G band at  $\sim 1580\text{ cm}^{-1}$ , and the 2D band at  $\sim 2680\text{ cm}^{-1}$  (Figure 1.3). The D band is induced by defects in the graphene lattice. It is not Raman active for pristine graphene but can be observed in samples with a high density of defects. The G band corresponds to in-plane vibration of  $\text{sp}^2$  carbon atoms which is the most prominent feature of most graphitic materials. Due to the increased quantities of carbon atoms contributing to the vibration mode, the G band becomes more intense with increasing graphene layers. Further, the shape, intensity and position are sensitive to charged impurities [16]. The 2D band is a second-order two-phonon mode and is very prominent in graphene as compared to bulk graphite [17]. The intensity ratio of the G and D band can be used to characterize the number of defects in a graphene sample [18]. The relative peak height of the G and 2D band serves to indicate the number of layers present for a graphite material. A significant change in both shape and intensity appeared as the number of layers increased. In monolayer graphene, the very sharp and symmetric 2D peak shows the intensity as twice higher as that of G peak, while in bulk graphite, the 2D band becomes broader, less symmetric, weak, and comprised of two components [19].

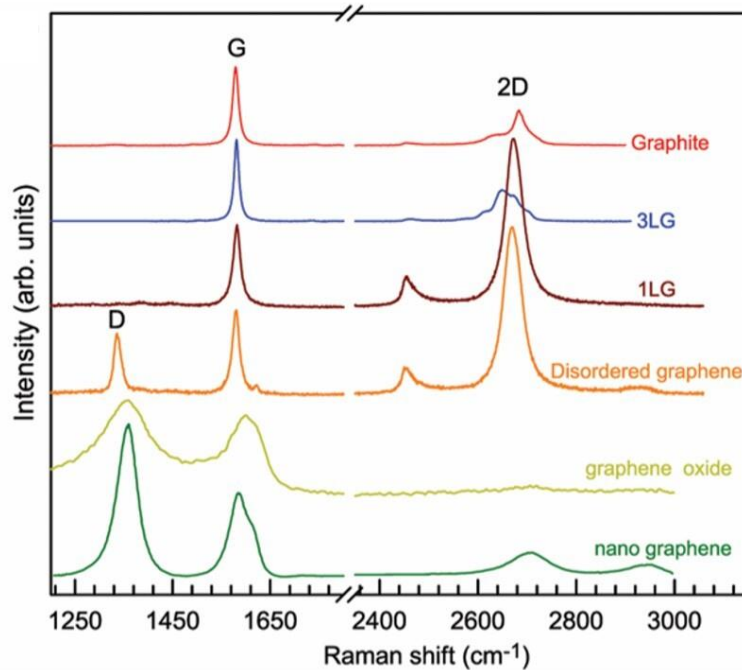


Figure 1.3. Raman spectra of graphene-based materials, including graphite, 1LG, 3LG, disordered graphene, graphene oxide and nanographene. (reproduced with permission from Ref [20])

### 1.1.2 Synthesis of graphene

After the initial discovery of graphene, the most exercised method to synthesize single-to-few layers graphene was the micromechanical cleavage of graphite, the now famous Scotch tape method, published by Geim and Novoselov in 2004. To date, there is almost no method that can match mechanical exfoliation for advanced graphene flakes in terms of high carrier mobility and low defect density graphene. However, it is an original top-down approach with neither high throughput nor high yield leading to limited scale production. So far, many alternatives to mechanical exfoliation are widely applied including bottom-up growth methods such as Thermal Decomposition of SiC and Chemical Vapor Deposition (CVD) method; chemical- or solvent-based exfoliation; graphene derivatives reduced, mainly graphite oxide (GO); and so on. Each of these approaches has its drawbacks.

### 1) Mechanical exfoliation

In the mechanical exfoliation method, also called the Scotch tape method, the highly oriented pyrolytic graphite (HOPG) works as a precursor, and graphite flakes are obtained by repeatedly peeling with scotch tape. The van der Waals attraction to the substrate can delaminate a single sheet when the scotch tape is lifted away. Geim and Novoselov were able to generate few- and single layer graphene flakes with dimensions of up to  $10\mu\text{m}$  [1]. Since the optical absorbance of graphene is just 2.3%, direct visual observation is impossible [21]. Therefore, these thin flakes were identified by optical microscopy with Si/SiO<sub>2</sub> wafer (300nm) as substrate, taking advantage of the change in refractive index between graphene and 300 nm thick silicon dioxide [1]. Observation showed high-quality flakes with sides of up to 1mm in length made by the subsequent group which were well-suited for fundamental research [22]. Though it produces highly quality graphene flakes, this method requires a great deal of patience as well as labors.



Figure 1.4. TEM image of micromechanical cleavage graphene film after electron-beam lithography and etching step. (reproduced with permission from Ref [23])

## 2) Thermal decomposition of silicon carbide

The synthesis of graphene by thermal decomposition of silicon carbide triggered by heating silicon carbide (SiC) to 1000-1500 °C high temperature in ultra-high vacuum causes the preferential sublimation of silicon from the SiC surface and subsequent graphitization of the remaining carbon atoms [24]. De Heer and Berger took the lead to produce few-layer graphene by thermal decomposition of SiC. The 6H-SiC single crystal was first tarnished by oxidation or H<sub>2</sub> etching aims to improve surface quality. The SiC source was heated in UHV to 1000 °C to remove the oxide layer followed by being heated to 1250–1450 °C, resulting in the formation of thin graphitic layers. Using this method, devices were produced with mobilities of 1100 cm<sup>2</sup> V<sup>-1</sup> s<sup>-1</sup> [25].

Hexagonal phase silicon carbide has been most commonly used for graphene synthesis. The promising cubic phase SiC also has attracted lots of attention [26]. This method leads to obtaining epitaxial graphene in which the thickness and carrier mobility of graphene flakes depends upon the size of the SiC wafers [27]. This method is potentially of interest to the transistor and semiconductor industry due to the capable for generating wafer-scale graphene layers and control of thickness [28]. However, huge challenges exist including the demanding growth conditions and weak anti-localization of graphene sheets obtained by this method. Further, similar to graphene obtained by peeling method, thermal decomposition of SiC displays extremely large, temperature independent mobility [29]. This technique offers high quality graphene but with a high production cost and low yield rate. Some modified methods that allow lower temperature conditions are in the progress. The nickel catalyzed growth can occur at 700–800 °C, where a thin layer of nickel is deposited on the surface of the SiC prior to annealing, and the final graphene film

growths on the upper nickel surface [30]. Despite the lower temperatures, the transition metal and graphene film transfer add additional cost.

### 3) Chemical vapor deposition

Chemical vapor deposition (CVD), in contrast to the thermal decomposition of SiC where carbon is already present, take advantages of the high temperature pyrolysis of gas formed carbon source on metal, has been widely used to grow large scale graphene films. The metal is used as both catalyst and substrate. Critical to the CVD method is a suitable catalyst or substrate surface to effectively dissociate the gaseous carbon precursor, promote graphene nucleation, crystal growth and domain merging [31].

Transition metals are known to be highly catalytically active thereby are the most suitable heterogeneous catalysts. Li et al. successfully produced large-scale monolayer graphene on copper foils. Raman spectroscopy and SEM imaging provide the evidence that graphene is primarily monolayer independent of growth time. This indicates that the process is surface mediated and self-limiting [32]. Zhang et al. reported the synthesis and Raman characterization of the formation of graphene on single crystal Ni and polycrystalline Ni substrates using chemical vapor deposition. A preferential formation of monolayer/bilayer graphene on the single crystal surface is observed. In contrast, CVD graphene formed on polycrystalline Ni leads to a higher percentage of multilayer graphene [33]. Fe [34], Ru [35], Co [36], Pt [37] are also widely used.

CVD method is promising for industrial applications due to its potential in producing large-area graphene films with high quality, high flexible and electrical conductivity [38]. However, the conventional method relies on the transfer of graphene films away from catalyst substrates onto desired target substrates, and usually include a chemical etching step, which not only increases the

production cost but also requires relatively long treatment cycles [39]. Applications where the catalyst or growth substrate forms part of the device structure is an attractive research direction.

#### 4) Sonication

Sonication is an effective exfoliation method to produce high-quality monolayer or few-layers graphene. Sonication is usually applied using an ultrasonic bath or ultrasonic probe, colloquially known as a sonicator. During the sonication, as the ultrasonic waves propagate through the medium, and molecules are pushed and pulled alternately due to the high- and low-pressure exerted by compression and rarefaction, respectively [40]. Microbubbles grow gradually until reach to an unstable state after few cycles then implode generating powerful shockwaves, produce normal and shear forces on graphite [41].

Liquid-phase sonication is significantly attractive due to the solubility of graphene in some certain solvents. The sonication process usually involves the preparation of dispersion of graphite, the exfoliation of dispersion via sonication and the purification of graphene [42]. During the dispersion step, appropriate surface energy solvent or surfactants are necessary to avoid the re-stacking of graphene since graphene tends to agglomerate in solvent due to the Van der Waals force. While the advantage is the possible avoidance of expensive and harmful solvents. In the exfoliate step, to increase the graphene output, simply increase of sonication time or a probe sonicator shows satisfactory results. It is worth noting that while prolonged sonication time improves the dispersibility of graphene and the final graphene yield, it is accompanied by a decrease in flake size and an increase in defect concentration [43]. And this method requires a large amount of energy since sonication is the only energy source.

#### 5) Reduction of graphite oxide

Graphene nanoflakes can also be obtained by reduction of graphite oxide (GO). The groups formed during the oxidation process, such as -OH group, render graphite oxide hydrophilic, enabling chemically exfoliation in several solvents, even water [44]. The GO suspension can initially be sonicated followed by deposition onto appropriate surfaces via spin coating or filtration. To produce graphene flakes, deposited GO are then reduced through a thermal or chemical method [45]. Graphene obtained by this method is suitable for applications in conductive inks, polymer fillers, sensors, energy devices such as battery electrodes and supercapacitors [46]. Reduction of graphene oxide has generally been preferred for graphene synthesis over exfoliation of graphite or expandable graphite, but the remaining oxygen groups and defects were found after the reduction process [47].

#### 6) Unzipping carbon nanotubes.

High quality graphene can be obtained from carbon nanotube by slicing since carbon nanotubes could be cut open to form two-dimensional graphene sheets in theory [48]. Monolayer or few-layer graphene can be synthesized by unzipping single or multi-walled carbon nanotubes respectively. This method results in a graphene sheet or ribbon with width dictated by the diameter of the carbon nanotube, while the slice width and edge types, armchair and zigzag, have significant influence on graphene properties [49]. Wet chemistry methods such as strong oxidizing agents or physical methods such as laser irradiation and plasma etching [50] are some common methods. However, given the novelty of the carbon nanotube precursor, the cost for commercial production is a concern. And due to the presence of oxygen defect sites, the resulting graphene flakes were electronically inferior to large-scale graphene sheets [51].

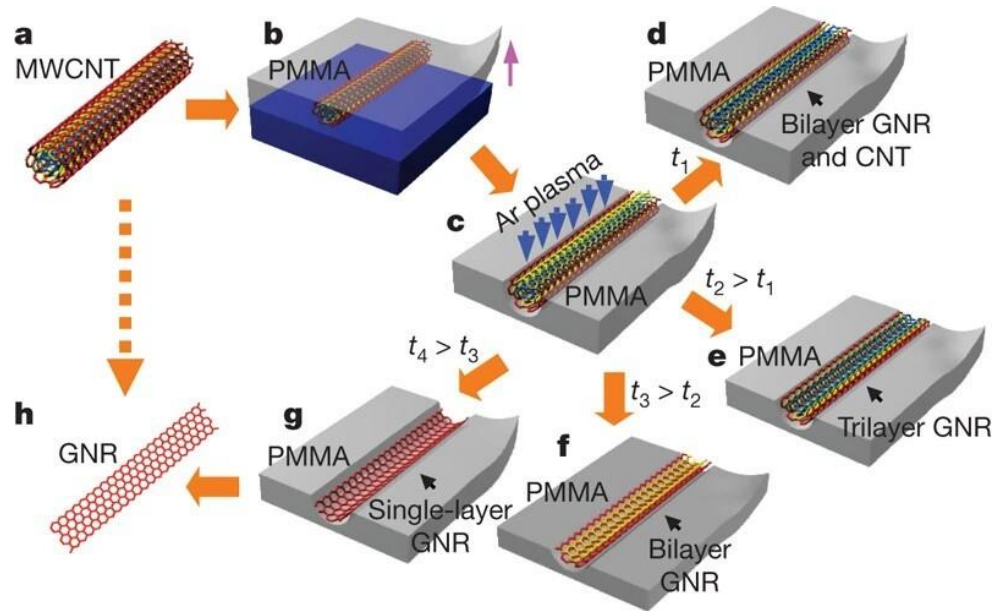


Figure 1.5. Unzipping multiwalled carbon nanotubes by plasma etching of nanotubes partly embedded in a polymer film. (reproduced with permission from Ref [50])

## 1.2 Graphene-based conductive inks

### 1.2.1 Motivation

In recent years, a tremendous interest in printed electronics has become evident. Printed electronics refers to the fabrication of electronic circuits and devices via printing technologies on various substrates such as paper [52], textile [53], and plastic [54]. It figures out the economic problems as well as the environmental problems compared to traditional manufacturing methods such as photolithography and vacuum deposition where complicated prefabrication process of templates or masks, high-cost equipment and environmentally undesirable chemicals are necessary. Undoubtedly, flexible printed electronics will play a major role in future electronic devices in the coming decades.

Until now, a number of available printing techniques have been developed to achieve high-performance, highly stable, low-cost and low waste electronic devices, such as inkjet printing,

screen printing, and gravure printing. Among these, inkjet printing has become the most favorable method for printed electronic applications. Inkjet printing is a type of computer-controlled deposition technique that recreates a digital image by propelling droplets of ink onto different substrates with liquid phase materials [55]. To date, the inkjet printing showed better flexibility in terms of the printing of the complex geometrical patterns with high spatial resolution. It can cope with wide range of layer thicknesses and line widths while maintaining higher edge sharpness of deposition. It facilitates the rapid fabrication process which a superiority over the templates based traditional printing method [56].

One major challenge of using graphene in flexible printed electronics is the ease and manufacturability of liquid-phase inks with appropriate viscosity and surface tension that results in rapidly and efficiently printing on the flexible substrates, while providing the required electrical and mechanical performance. Up to now, multiple types of conductive inks have been developed for the formation of printed patterns including metal-based inks, conductive polymer inks and carbon-based inks, but with infancy especially in the graphene nano-ink area.

Other challenges and opportunities should also be learned from experience with metal nanoparticle conductive inks. Firstly, nanoparticles should be stable against aggregation and precipitation. Metal nanoparticles have been widely used in large scale dispersion with stabilizing agents, which meets the requirements for ink formulation and printing quality, via the wet chemical methods. Among them, silver-based inks are the most favored metal inks and are under rapid development for applications in printed flexible electronics due to their excellent electrical properties. However, the high cost, low concentration, and unstable performance in electromigration limit their widespread industrial applications [57], which makes copper an ideal alternative since its abundance and comparable bulk conductivity. However, copper nanoparticles

are easily oxidized both under ambient condition and at high processing temperature which reduces the electrical conductivity [58,59]. Another challenge is the obligatory post-printing processes such as sintering that remove stabilizing agents and other ink components while improving the nanoparticles physical contacts [60].

Conducting polymer is a popular conductive ink material based on the high voltage window, high conductivity in a doped state, with possessing high energy storage capacity and with low environmental impact [61]. But the apparent disadvantages such as low stability according to the swelling and shrinking of conducting polymer hinders the application of printed conducting polymer electronics due to mechanical degradation [62]. To mitigate the influence of low stability, improving the morphologies of conducting polymer materials via composites materials has been suggested.

Graphene stands out from other carbon fillers due to the large surface area. The ideal graphene sheets are supposed to be highly ordered with outstanding surface areas ( $2630 \text{ m}^2 \text{ g}^{-1}$ ), high thermal conductivity ( $5000 \text{ W mK}^{-1}$ ), high electron mobility ( $2.5 \times 10^5 \text{ cm}^2 \text{ V}^{-1} \text{ s}^{-1}$ ), strong chemical durability and high Young's modulus (1 TPa) [63]. Graphene-based materials are promising building blocks in nanotechnology, due to the potential in various applications based on the outstanding properties discussed above. As shown in Figure 1.6, the high surface area and high electrical conductivity of graphene contributes to an outstanding performance in ultracapacitors. The high electron mobility and ambipolarity of graphene, where the nature of a charge carrier changes at the Dirac point with the requisite gate bias, enables the successfully application of dual-gated field effect transistors. Graphene can also be used to fabricate flexible transparent devices due to the low sheet resistance and high transparency. Besides, graphene materials have potential applications in rechargeable lithium ion batteries due to the high storage capacity; in optoelectronic

devices such as solar cells, owing to the unique optical and electrical properties of graphene [64]. It is desirable to harness the remarkable properties of graphene and its derivatives in conductive inks for printed electronics.

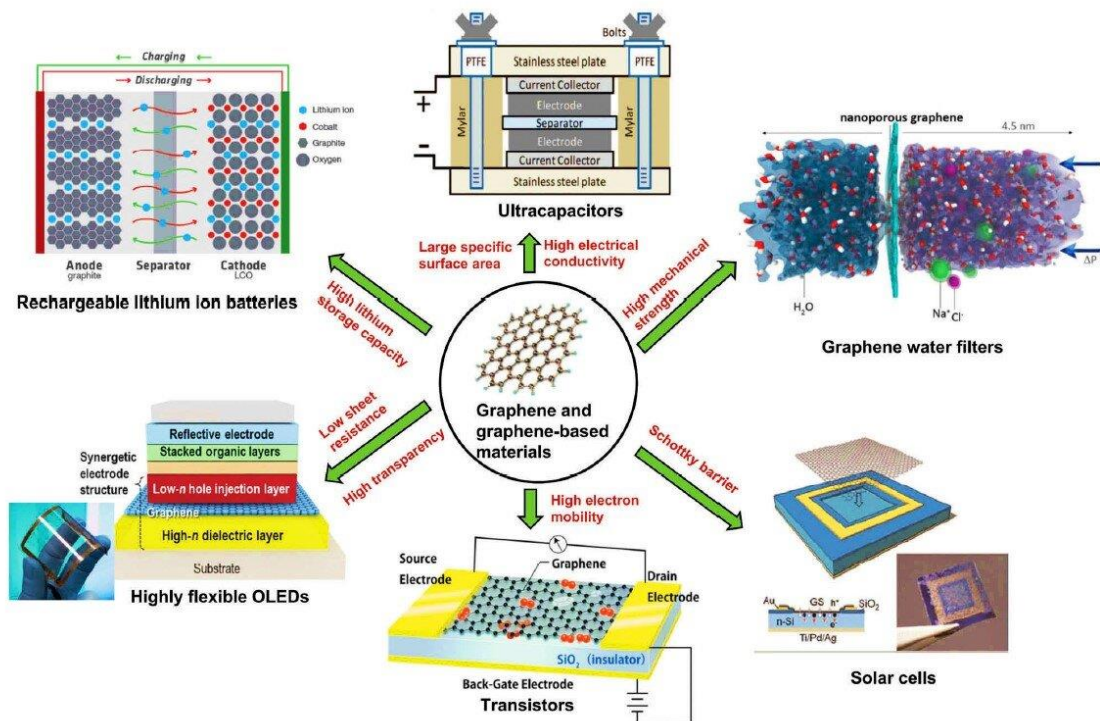


Figure 1.6. Applications of graphene and graphene-based materials. (reproduced with permission from Ref [64])

### 1.2.2 Synthesis of graphene conductive inks

The most common method adopted for graphene production includes the bottom-up methods, such as thermal decomposition of silicon carbide and chemical vapor deposition, forming large-scale and thickness controllable graphene; and top-down methods such as reduction of graphene oxide. However, the former techniques are limited by restricted dimensions and high cost resulting in products that cannot meet the requirement for high volume commercial

applications. The original method of mechanical exfoliation is only good for fundamental studies but without large scale manufacturing and applications. However, a cheaper and high throughput method of producing graphene is desirable number of applications such as electrochemical energy and sensing. From Figure 1.7, it is obvious that liquid phase exfoliation method can obtain a stable dispersion of graphene compared with all the above methods, which only involves the exfoliation of graphite or graphite related materials via sonication high-shear mixing [65]. Therefore, liquid phase exfoliation is a viable method for manufacturing of conductive ink area.

Here, we focus on liquid phase exfoliation by sonication. Sonication is usually applied with ultrasonic bath or ultrasonic probe, colloquially known as a sonicator. During the sonication, as the ultrasonic waves propagate through the medium, molecules are pushed and pulled alternately due to the high- and low-pressure exerted by compression and rarefaction, respectively [40]. Microbubbles grow gradually until reach to an unstable state after few cycles then implode generating powerful shockwaves, produce normal and shear forces on graphite [41]. The liquid phase exfoliation process usually involves dispersion of graphite, exfoliation of dispersion and purification. During the dispersion, appropriate surface energy solvent or surfactants are necessary to avoid the re-stack of graphene since graphene tends to agglomerate in solvent due to the Van der Waals force. In the exfoliation step, to increase the graphene output, simply increase of sonication time or a probe sonicator shows satisfactory results. It is worth noting that while prolonged sonication time improves the dispersibility of graphene and the final graphene yield but accompanied by a decrease in flake size and an increase in defect concentration. After exfoliation, the solvent-graphene interaction needs to balance the inter-sheet attractive forces. Therefore, appropriate solvent is significant important for graphene inks, that minimize the interfacial tension between the liquid and graphene flakes [66].

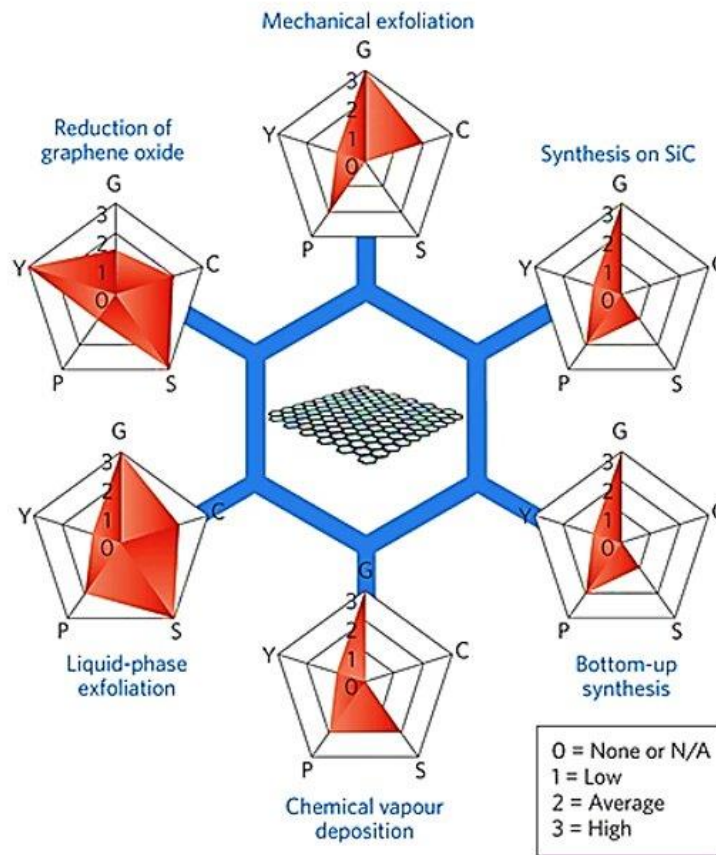


Figure 1.7. Graphene produce methods with evaluation in terms of quality (G), yield (Y), cost aspect (C; a low value corresponds to high cost of production), purity (P) and scalability (S). (reproduced with permission from Ref [65])

Based on the different starting graphite sources, the liquid phase exfoliation process can be generally classified into three main categories: liquid-phase exfoliations from graphite oxide, pristine graphite, and expanded graphite.

### 1) Liquid phase exfoliation of graphite oxide

Reduction of graphene oxide is one of the most versatile approach which offers the greatest ease for functionalization. Graphene oxide can be easily exfoliated from graphite oxide which can

be prepared by the Brodie [67] or Hummers method [68]. Brodie used potassium chlorate ( $\text{KClO}_3$ ) combined with nitric acid ( $\text{HNO}_3$ ) to oxidize graphite, the oxide process of Hummers method involves potassium permanganate ( $\text{KMnO}_4$ ) and sulfuric acid ( $\text{H}_2\text{SO}_4$ ). The subsequently reduction with reducing agents, such as hydrazine, sodium borohydride, and lithium aluminum hydride, aims to remove the oxygen-based functional groups in the system [69]. Liquid phase exfoliation of graphite oxide has undoubted advantage, the  $\text{sp}^2$ -bonded carbon structure of graphene is occupied by few of hydrophilic groups, such as hydroxyl and carboxyl groups, which makes graphite oxide soluble in most solvents. At the same time, those hydrophilic groups can be used to covalently and non-covalently attach functional units to this 2D scaffold, results in changes in both chemical and physical properties [70]. However, the resulting graphene sheets have remaining oxygen groups and significantly increased defects compared with pristine graphene sheets, which disrupt the band structure and compromise the outstanding electronic properties [71]. And even though reducing agents have been extensively used towards obtaining graphene sheets, some of them has significant drawbacks such as the highly toxic of hydrazine and the inert atmosphere needed for lithium aluminum hydride.

## 2) Liquid phase exfoliation of pristine graphite

To minimize the oxide defects in graphene, liquid phase exfoliation of pristine graphite is a great choice. However, the van der Waals attraction among adjacent graphene sheets is still a huge challenge for the complete exfoliation into individual layers, even though adjacent graphene sheets can slide along the perpendicular direction. Two main routes for obtaining stable dispersion from pristine graphite are dispersion in organic solvents and dispersion in aqueous medias with dispersants such as surfactants.

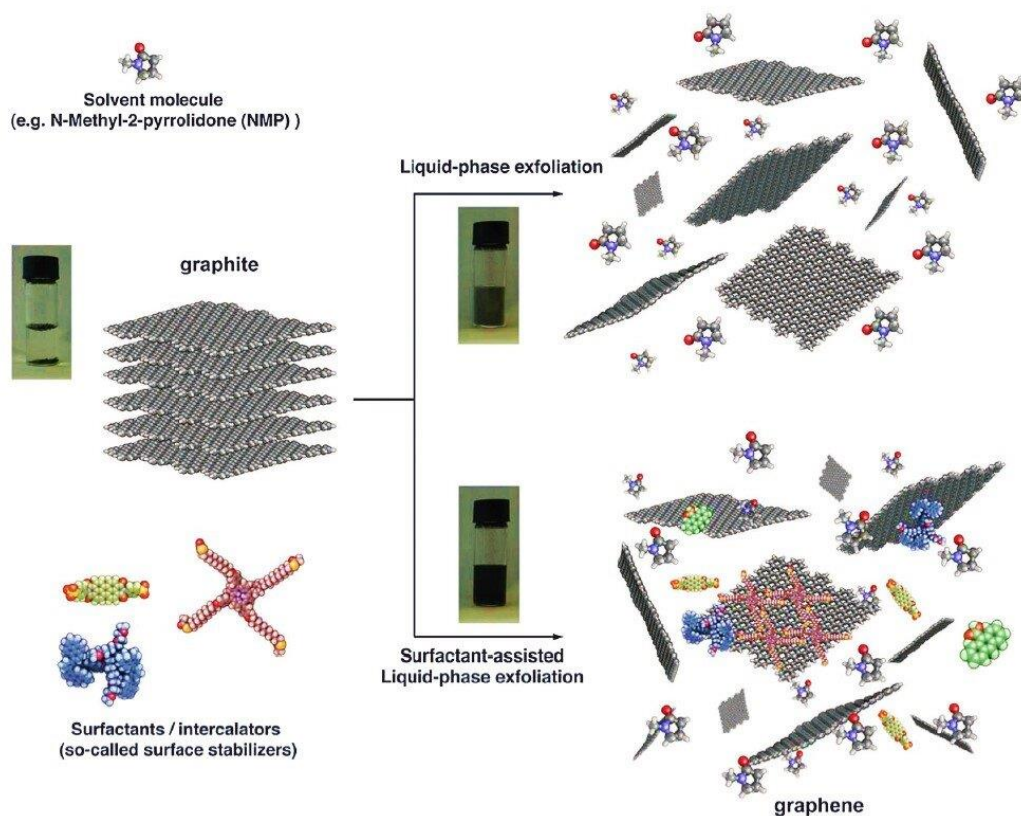


Figure 1.8. Liquid-phase exfoliation process of graphite in the absence and presence of surfactants. (reproduced with by permission from Ref [72])

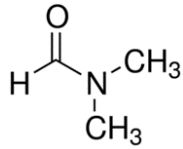
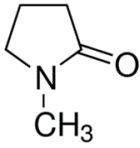
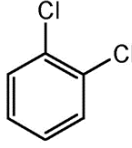
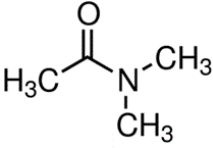
### 2.1) Exfoliation in organic solvents

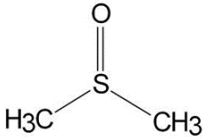
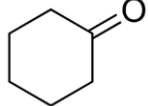
One of the most straightforward and effective methods to overcome the van der Waals interaction between the graphene layers held within a  $\pi$ - $\pi$  stacking is liquid immersion, where the interfacial tension plays a key role [73]. The high interfacial tension between material and solvent results in poor dispersibility of the material. Graphitic flakes tend to agglomerate in solution with high interfacial tension [74]. A range of solvents with varying surface tension were used for graphite exfoliation, a peak for the concentration of resulting graphene appeared at surface tension around  $40 \text{ mJ m}^{-2}$ , which matched with the reported surface energy value of graphite [75]. Therefore, solvents with surface tension  $\gamma \sim 40 \text{ mJ m}^{-2}$  are the best for the dispersion of graphitic

flakes due to the minimized interfacial tension between graphene and solvent. So that the liquid phase exfoliation of pristine graphite in organic solvents or ionic liquids is facile. The surface tension of some common organic solvents can be found in Table 1.1.

Unfortunately, most of organic solvents such as N-methyl-2-pyrrolidone (NMP), N,N-dimethylformamide (DMF), and ortho-dichlorobenzene (ODCB) are relatively expensive and toxic. Meanwhile, the high boiling point limits their viability for real manipulation since the presence of remaining solvent can greatly impact the device electrical performance.

Table 1.1. Surface tension, boiling point and chemical structure of some common organic solvents.

| Organic solvent                 | Surface tension<br>(mJ m <sup>-2</sup> ) | Boiling point<br>(°C) | Chemical structure  |
|---------------------------------|--|-----------------------|---|
| N,N-Dimethylformamide<br>(DMF)  | 37.1                                     | 153                   |  |
| N-Methyl-2-pyrrolidone<br>(NMP) | 40                                       | 203                   |  |
| Ortho-dichlorobenzene<br>(ODCB) | 37                                       | 181                   |  |
| N,N-dimethylacetamide<br>(DMAC) | 36.7                                     | 165                   |  |

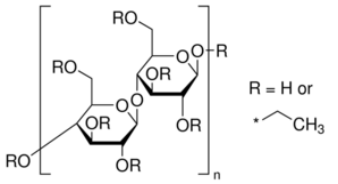
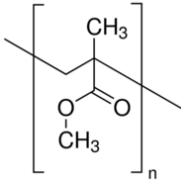
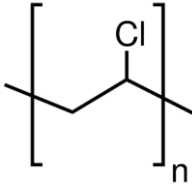
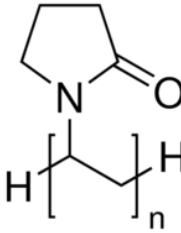
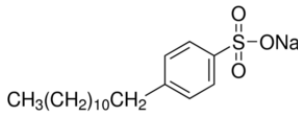
|                             |      |     |   |
|-----------------------------|------|-----|---|
| Dimethylsulfoxide<br>(DMSO) | 42.9 | 189 |  |
| Cyclohexanone               | 35.1 | 156 |  |

## 2.2) Surfactants-assisted exfoliation

Due to the subsequent processing and environmental problems, exfoliation of pristine graphite in low boiling solvents is preferable. However, most low boiling solvents, such as water ( $72.8 \text{ mJ m}^{-2}$ ) and ethanol ( $22.1 \text{ mJ m}^{-2}$ ), have an unsuitable surface tension for the direct exfoliation. Surfactants can promote the exfoliation of graphite into graphene, particularly when such a compound has a high energy of adsorption on the basal plane of graphene [76]. Adsorption of these surfactants onto the graphene surface occurs through  $\pi$ - $\pi$  interactions between the planar  $\pi$ -conjugated surfaces, by reducing the surface free energy of the dispersion [77]. Some conventional surfactants used for the exfoliation of pristine graphite in water and other low surface tension solvents are shown in Table 1.2.

However, the disadvantage in using surfactants to assist the liquid phase exfoliation of pristine graphite is the remaining surfactants. Regardless of the manufacturing method, the resulting devices consist of material including graphene flakes, surfactants, residuals of solvents, which can be problematic in the field of electronics. It is therefore significant important to remove residuals from liquid phase exfoliated graphene-surfactant composites by post process.

Table 1.2. Chemical structure of some common surfactants.

| Surfactants                 | Chemical structure   | Surfactants                           | Chemical structure  |
|-----------------------------|--|---------------------------------------|---|
| Ethyl cellulose (EC)        |   | Polymethyl methacrylate (PMMA)        |  |
| Polyvinylchloride (PVC)     |   | Polyvinylpyrrolidone (PVP)            |  |
| Sodium dodecylsulfate (SDS) | $\text{CH}_3(\text{CH}_2)_{10}\text{CH}_2\text{O}-\text{S}(=\text{O})_2\text{ONa}$ | Sodium dodecylbenzenesulfonate (SDBS) |  |

### 3) Liquid phase exfoliation of expanded graphite

In natural graphite, the bonding force between the parallel graphene sheets is weak van der Waals forces. The spacing between the natural graphene sheets can be appreciably opened to provide a marked expansion. High temperature or microwave treatments have been applied to produce expand graphite which can be used as an origin liquid-phase exfoliation material. More or less, this method utilizes the concept of graphite intercalation compound, which has been widely used for industrial exfoliated graphite [78]. Qian et al. reported a solvothermal-assisted exfoliation method to produce monolayer and bilayer graphene with a highly polar organic solvent, acetonitrile (ACN) and expanded graphite as the starting material. Figure 1.9. illustrates the solvothermal-assisted exfoliation and dispersion process. The graphite was heated at 1000 °C to obtain the expanded graphite. Subsequently, the expanded graphite was mixed with ACN in a

Teflon autoclave and heated, ACN molecules were introduced into the interlayers by a solvothermal process. Upon sonication, monolayer and bilayer graphene sheets were peeled off from expanded graphite and stably dispersed in ACN.

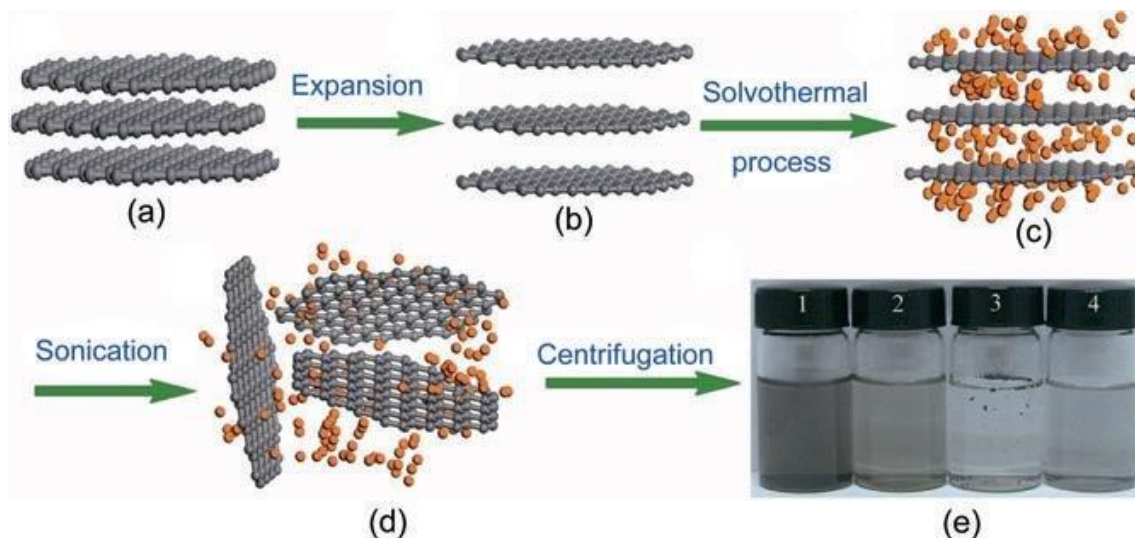


Figure 1.9. Schematic illustration of solvothermal-assisted exfoliation and dispersion of graphene sheets in ACN. (reproduced with permission from Ref [79])

### 1.3 Recent progress of graphene-based conductive inks

#### 1.3.1 Classification of graphene-based conductive inks

##### 1) Graphene oxide inks.

Le et al. [80] produced 0.2 wt.% water-based graphene oxide ink for the fabrication of electrically conductive graphene electrodes by inkjet printing with subsequent thermal reduction. Graphene oxide ink was observed to be dispersion-stable for months due to the presence of hydrophilic functional groups. The viscosity and surface tension of the graphene oxide ink were 1.06 mPa s and 68 mN.m<sup>-1</sup> respectively at room temperature. The electrochemical performance of

inkjet-printed graphene electrodes compared favorably to those electrodes fabricated by traditional methods.

Porro et al. [81] prepared a water-based graphene oxide/poly (ethylene glycol) diacrylate (PEGDA) ink. Graphene oxide aqueous dispersion with a concentration about  $4 \text{ mg ml}^{-1}$  were prepared using high-speed ultraturrax and ultrasonic bath. PEGDA was added to the water-based graphene oxide dispersion then, the final concentration of graphene oxide relative to the PEGDA matrix is 4 wt.%. The network clusters of reduced graphene oxide inside the polymer matrix act as preferential pathways for the mobility of charge carriers, thus results in the decreased resistivity after UV irradiation.

Dua et al. [82] described a flexible and lightweight resistor made of a reduced graphene oxide thin film, which was inkjet-printed onto flexible plastic substrates using surfactant-assisted graphene oxide ink and vitamin C as reducing agent. Ascorbic acid powder was added to aqueous graphene oxide dispersion and heated to  $80 \text{ }^\circ\text{C}$ , at which point the color changes from brown to black, signaling the conversion into reduced graphene oxide platelets. RGO ink was formed with Triton-X100 as a surfactant. The resulting film has fewer defects and better electrical conductivity properties compared to films obtained by hydrazine-based reduction process.

Recently, Overgaard et al. [83] developed a scalable water-based graphene oxide ink used in screen-printed flexible electric circuit. Devices were subsequently reduced with a 1:1 mixture of trifluoroacetic acid and hydroiodic acid at low temperature. This post-printing chemical reduction outperforms high temperature annealing. The dry content of the graphene oxide ink was determined around  $30 \text{ mg ml}^{-1}$ . The reduced prints exhibit low sheet resistance of  $327 \text{ } \Omega \text{ sq}^{-1}$  for thin semitransparent layers with 37% transmittance.

## 2) Graphene inks

Paton et al. [84] produced a stable graphene-based ink via liquid-phase shear-exfoliation of graphite in N-methylpyrrolidone (NMP). The graphene produced in this way is virtually indistinguishable from that produced by liquid-phase sonicate-exfoliation of graphite and has been demonstrated to be useful in a range of applications from composites to sensors. However, NMP is not environmentally benign.

Lee et al. [85] prepared a highly stable graphene ink consists of graphene nanosheets and sodium n-dodecyl sulphate (SDS). The graphene ink can be stable for more than one month due to SDS which prevents the aggregation of graphene nanosheets. Conductive features were fabricated on a flexible PI film by inkjet printing. With higher number of printing cycles, the loading weight of graphene nanosheets on PI film showed a linear increase. The conductivity of the sintered film where excess SDS were effectively removed, was improved to  $121.95 \text{ S m}^{-1}$  via a post-heating process.

Chang et al. [86] combined the hydrophilic N-doped graphene with the PVA- $\text{H}_3\text{PO}_4$  gel electrolyte to assemble a stabilized water-soluble graphene@PVA- $\text{H}_3\text{PO}_4$  hybrid ink formulation. The improved accessibility of electrolyte ions to the active surfaces of graphene in the printed microelectrodes leads to the enhanced electrochemical performance.

Gao et al. [87] developed a stable pristine graphene ink where the pristine graphene was produced by exfoliating pristine graphite using an ultrasound-assisted supercritical  $\text{CO}_2$  based method as shown in Figure 1.10. The graphene ink was formulated with cyclohexanone and ethyl cellulose (EC), as the solvent and surfactant. The ink, at concentrations up to  $1 \text{ mg ml}^{-1}$ , was stable for more than 9 months and had compatible fluidic characteristics for efficient and reliable inkjet printing. The conductivity of the inkjet-printed films after 30 printing passes up to  $9.24 \times 10^3 \text{ S m}^{-1}$ , and the films had a transmittance of approximately 60% after annealing.

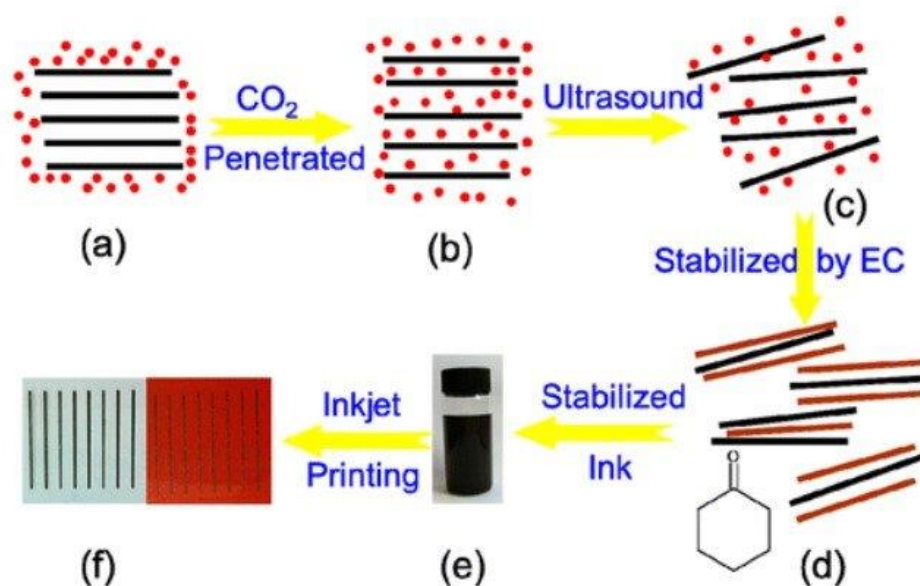


Figure 1.10. Schematic illustrates the preparation process of pristine graphene ink and its printed electrodes. (reproduced with permission from Ref [87])

### 3) Graphene/polymer hybrid ink.

Graphene/polyaniline hybrid materials can address the shortcomings of polyaniline and form an underlying stable conductive network due to the incorporation of graphene. Xu et al. [88] prepared graphene/polyaniline ink by liquid phase sonication of graphite powder and polyaniline in water with SDBS as surfactant. and fabricate graphene/polyaniline thin film electrodes. Inkjet printing technology is then used to produce graphene/polyaniline thin-film electrodes which exhibited conductivity of  $0.29 \text{ S cm}^{-1}$  after annealing. Electrochemical measurements of the supercapacitor fabricated by these thin-film electrodes with a  $1 \text{ M H}_2\text{SO}_4$  electrolyte yield a maximum specific capacitance of  $82 \text{ F g}^{-1}$ , power density of  $124 \text{ kW kg}^{-1}$  and energy density of  $2.4 \text{ Wh kg}^{-1}$  when a scan rate of  $20 \text{ mV s}^{-1}$  is applied.

Seekaew et al. [89] formulated graphene–poly (3,4-ethylenedioxythiophene): poly (styrene sulfonate) (PEDOT:PSS) hybrid inks for fabricating innovative flexible ammonia gas sensors. The hybrid inks were synthesized by ultrasonication bath of graphene powder, PEDOT:PSS solution, dimethyl sulfoxide (DMSO), ethylene glycol and Triton X-100. Here, DMSO was used as the primary solvent that exhibits good conductivity and low baseline resistance at room temperature, while EG and Triton X-100. were added to improve of the viscosity and surface tension as well as to prevent of rapid drying during printing. The final graphene–PEDOT:PSS solution contains 2.33 wt.% of graphene to the total solid content of PEDOT:PSS. And it was demonstrated that  $\pi$ – $\pi$  interactions occurred between graphene and PEDOT:PSS. The ink-jet printed graphene–PEDOT:PSS gas sensor exhibits high response and high selectivity to ammonia in a low concentration range of 25–1000 ppm at room temperature. The sensing performance may be attributed to the high specific surface area of graphene and enhanced interactions between the sensing films and ammonia molecules via  $\pi$  electrons network.

#### 4) Graphene/metal hybrid inks

Pan et al. [90] fabricated a novel electrochemical graphene/gold-based biosensor for the detection of bisphenol A. The graphene/gold hybrid ink was prepared by sonication-assisted dispersing of graphene oxide and chloroauric acid ( $\text{HAuCl}_4$ ) in water, followed by microwave heating and thermally incubation. The biosensor was prepared by the simple classic casting method onto glassy carbon electrodes and exhibited excellent performance for BPA determination with a wide linear range ( $2.5 \times 10^{-3} - 3.0 \mu\text{M}$ ), a highly reproducible response (RSD of 2.7%), low interferences and long-term stability.

Jabari et al. [91] developed a graphene/silver nanoparticles hybrid ink which can be used to print highly conductive and flexible graphene/Ag electronics by aerosol-jet. Graphene was

obtained by chemical exfoliation of natural graphite flakes in ethanol using sonication in the presence of ethyl cellulose as a stabilizer. The graphene/EC powder were then dissolved in a ethanol and terpineol system followed by a filter process, and mixed with Ag nanoparticle solution in a volume ratio of 3:1. The printed graphene/Ag nanoparticles features displayed the enhanced electrical conductivity of  $1.07 \times 10^{-4} \Omega \text{ cm}$  after annealing, about 100 times less resistivity when compared to graphene patterns.

Xu et al. [92] prepared a hybrid conductive ink consists of Ag nanoparticles (15 wt.%) and graphene–Ag nanosheets (0.15 wt.%) for writing electronics on paper. The Ag nanoparticles and graphene–Ag composites were dispersed in ethanol, ethylene glycol and glycerol, added with a ratio of 50:45:5 vol%. Ethylene glycol and glycerol aim to adjust the ink viscosity. The electrical conductivity of graphene was enhanced, due to the decreased contact resistance caused by the graphene junctions by depositing Ag nanoparticles (NPs) onto graphene sheets. A typical resistivity value measured was  $1.9 \times 10^{-7} \Omega \text{ m}$ , which is 12 times less compared with bulk silver. Even after thousands of bending cycles or rolling, the resistance values of the written tracks only increased slightly.

### **1.3.2 Devices and applications**

#### 1) Electronic devices and energy devices

Liu et al. [93] developed a novel fabrication of large area conductive graphene films by spray-coating of graphene/PEDOT:PSS hybrid inks. Graphene films exhibited excellent electrical and mechanical properties, thus enable their application in ultrathin organic photodetectors (OPD) with performance comparable to that of the state-of-the-art Si-based inorganic photodetectors. Conductive graphene films with thicknesses between 10 and 20 nm yields a conductivity of about

1000 S cm<sup>-1</sup> with a transmittance of 80% at 500 nm. The work shows the potential for the future development of transparent electrodes for optoelectronics, and other emerging flexible devices.

Hyun et al. [94] successfully prepared paper-based foldable electronic circuits via vacuum filtration of graphene dispersion and a simple transfer process with a pen. Without demand for special equipment, the dimensions of graphene membranes including width and thickness can be easily controlled by the vacuum filtration. Foldable electronic circuits were then fabricated by selective transfer of graphene patterns onto a paper from the filter membrane without the need of a printing mask. The employed surfactant PSS (polystyrene sulfonate) in graphene ink resulting in stable dispersion, and hydrophilic surface on the graphene nanoplates, enabled a clear selective transfer process and a favorable adhesion between the graphene and the paper substrate. The resulting conductive circuits showed excellent folding stability with small decrease of conductance at any folding angles from -180° to 180°. They also demonstrated a potential application of foldable circuit board in light-emitting diode (LED) chips array.

Wei et al. [95] produced solid-state flexible lithium batteries based on graphene inks through a scalable and versatile printing method. The batteries consist of a lithium foil (anode), a graphene hybrid inks printed current collector (cathode) and the polymer-based gel electrolyte between them. Graphene was fabricated by chemical reduction of exfoliated graphene oxide and modified by polystyrene sulfonate (PSS). Electrodes using modified graphene inks containing anatase titanate (TiO<sub>2</sub>) nanoparticles show improved performance over pristine graphene ink as well as the PSS modified one. The assembled solid-state flexible lithium batteries showed excellent performance with specific capacity of up to 582 mA h g<sup>-1</sup>.

Casaluci et al. [96] demonstrated a large-area dye-sensitized solar cell module based on a spray-coated graphene ink counter electrode. Graphene-based ink was prepared by liquid phase

exfoliation of graphite in dimethylformamide. By using a spray-based coating method they deposited the graphene ink on a transparent conductive oxide substrate to prepare a large area counter-electrode ( $43.2 \text{ cm}^2$  active area) with a transparency of 44%, which was then successfully integrated in a large-area dye-sensitized solar cell module achieving a power conversion efficiency of 3.5%.

Li et al. [97] demonstrated a route for the fabrication of all-solid-state flexible supercapacitors and micro-supercapacitors using a pristine graphene ink by solution casting and inkjet printing. The solid-state flexible devices exhibit high volumetric capacitance, promising energy and power densities, and excellent cycling stability and mechanical durability, with a volumetric device capacitance up to  $17.8 \text{ F/cm}^3$ . Li et al. [98] proposed a simple full-inkjet printing technique for the fabrication of graphene-based micro-supercapacitors (MSCs) on various substrates in a scalable manner. High-performance graphene inks were formulated with electrochemically exfoliated graphene with a solvent exchange technique. To solve the problem of the toxicity and low viscosity of DMF that used for exfoliation, the mixture of cyclohexanone and terpineol were used for final graphene inks, the so-called solvent exchange technique. Along with the printed polyelectrolyte, poly (4-styrenesulfonic acid), the fully printed graphene-based MSCs attain the highest areal capacitance of  $0.7 \text{ mF/cm}^2$ , substantially advancing the state-of-art of all-solid-state MSCs with printed graphene electrodes. They also stated that without any extra protection or encapsulation, the large-scale MSCs array, composed by more than 100 devices on silicon wafers or Kapton, can be reliably charged up to 12 V and retain the performance even 8 months after fabrication.

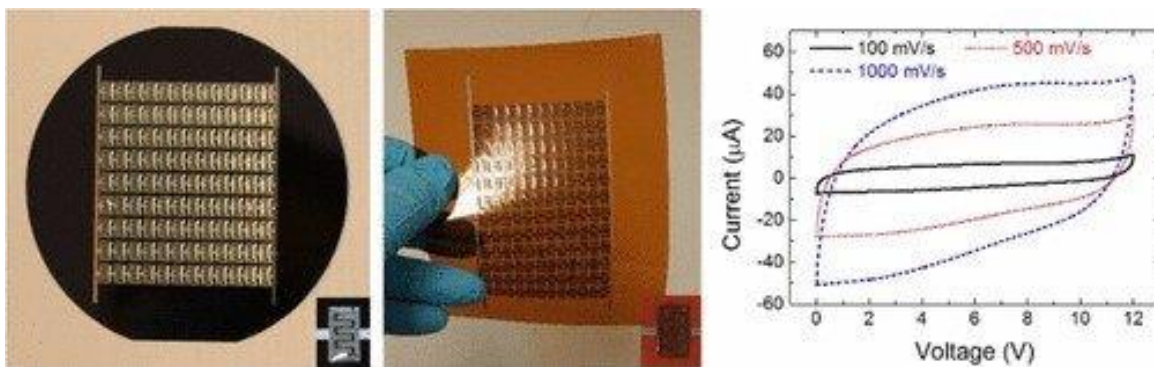


Figure 1.11. Photographs of a  $12S \times 12P$  MSC array on silicon wafer (a) and Kapton (b). (C) CV profiles of the  $12S \times 12P$  MSC array at different scan rates with a voltage window of 12 V. (reproduced with permission from Ref [98])

## 2) Electrochemical sensors

Dua et al. [82] reported a sensitive flexible sensor fabricated by reduced graphene oxide (rGO)-based inks. The rGO films were achieved by the reduction of printed GO using ascorbic acid as a mild and green reducing agent, which were used to detect chemically aggressive vapors such as  $\text{NO}_2$  and  $\text{Cl}_2$ . Vapors in the 100 ppm – 500 ppb concentration range can be detected in an air sample without the aid of a vapor concentrator.

Meng et al. [99] produced reduced graphene oxide (rGO) modified  $\text{Cu}_2\text{O}$  nanorods via a two-step synthesis method. In the first step,  $\text{CuO}$  rods were prepared in graphene oxide solution using cetyltrimethyl ammonium bromide as a soft template by the microwave-assisted hydrothermal method, graphene oxide was reduced simultaneously.  $\text{Cu}_2\text{O}$  nanorods/rGO composites were achieved by the annealing of resulting composite in the first step. The  $\text{Cu}_2\text{O}$ /rGO composites-based sensor exhibited an excellent sensitivity and selectively, as well as linear response toward  $\text{NH}_3$  at room temperature. A fitting curve of the sensor response versus the  $\text{NH}_3$  concentration in the range of 100 – 500 ppm could be easily obtained.

Ali et al. [100] proposed a highly sensitive humidity sensor consisted of silver interdigital electrodes and graphene/methyl red composite layer, for the potential wearable electronic applications. The silver interdigital electrode was fabricated on a low cost transparent polyethyleneterephthalate (PET) substrate through commercialized inkjet printer, graphene/methyl red composite was then deposited over the silver printed interdigital electrodes via electrohydrodynamic jet printing technology with thickness about 300 nm, to achieve a high sensitivity and wide sensing range. The electrical resistance of the sensor inversely varies from 11 M $\Omega$  to 0.4 M $\Omega$  against the relative humidity content from 5% to 95%. Besides, the resistive and capacitive sensitivity of the sensor against humidity was 96.36% and 2,869,500%, respectively. The response and recovery time of the proposed sensor is 0.251s and 0.35s, respectively.

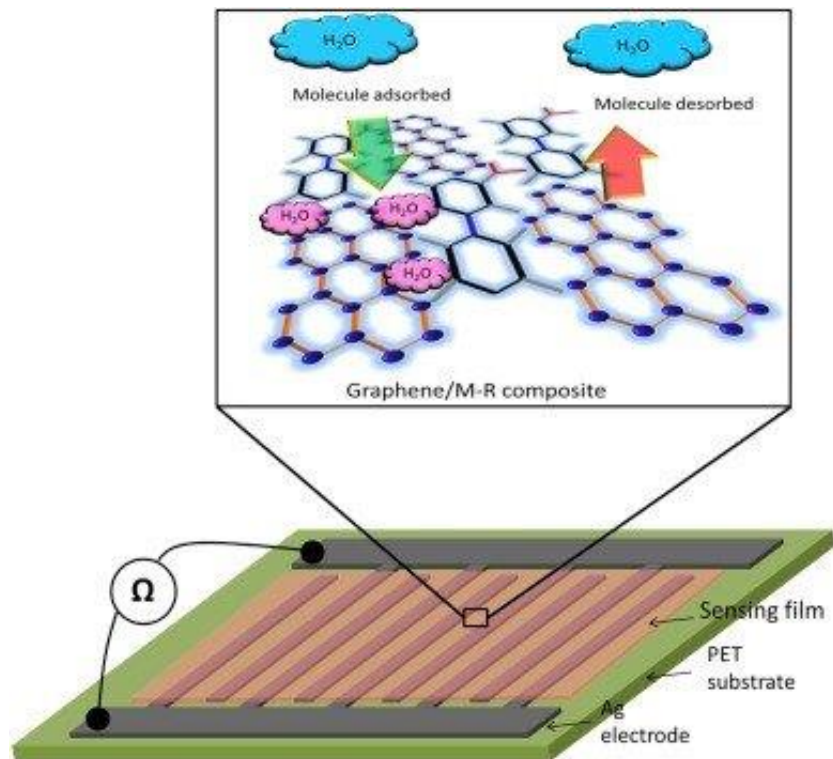


Figure 1.12. Schematic representation of the proposed humidity sensor. (reproduced with permission from Ref [100])

### 3) Biochemical sensors

Kanso et al. [101] integrated a new screen-printed graphene electrode in one channel flow-cell for enzymatic sensors, with an improved analytical response and enhanced electroactive area of up to 388% over a standard electrode. To study the entrapped cellobiose dehydrogenase from the ascomycete *Corynascus thermophilus* (CtCDH), CtCDH-PVA-modified graphene electrodes were fabricated, which showed same initial activity during 8 h and good storage stability with a only 9% decrease in analytical response after 3 months storage at 4 °C. A wide linear measurement ranging between 0.25 and 5 mM were achieved with the calibration curve of lactose using optimized parameters.

Labroo et al. [102] demonstrated graphene ink-based biosensor arrays on a microfluidic paper for the multiplexed detection of different metabolites. A fast, sensitive, and synchronous detection for different metabolites such as glucose, lactate, xanthine and cholesterol can be observed. The device exhibits a fast measuring time of less than 2 min, a low detection limit of 0.3  $\mu\text{M}$ , and a dynamic detection range of 0.3–15  $\mu\text{M}$ . The approach may open new avenues for a variety of applications in healthcare, pharmaceuticals, food science, and environmental monitoring.

## 1.4 Outline of the thesis

This thesis describes an approach for graphene ink development for integration in printed devices. Chapter 2 outlines the process steps involved in formulating the graphene ink in a way that could be readily used for printed electronics, including electrochemical sensors and energy storage devices. The optimization of graphene ink formulation was studied by Ultraviolet–visible spectroscopy and the electrical resistance characterization. Chapter 3 describes the development of hybrid or composite graphene inks for printed electronics by adding graphene aerosol gel and

multi-walled carbon nanotubes, respectively. The electrochemical performance of graphene-based inks was studied by cyclic voltammetry method.

## Chapter 2 - Synthesis and optimization of graphene conductive inks

The goal of the present chapter is to describe the process steps involved in formulating the graphene ink in a way that could be readily used for printed electronics, including electrochemical sensors and energy storage devices in wide range of substrate materials. The materials presented in this chapter constitute part of a non-provisional PCT application (Kansas State University Disclosure Number 2019-066), filed on June 25, 2020, as follows.

*“Nano-inks of Carbon Nanomaterials for Printing and Coating, PCT Application No.: PCT/US2020/039547”*

### 2.1 Formulation of graphene inks

In this chapter, the preparation of graphene conductive inks via surfactant-assisted liquid phase exfoliation and solvent exchange technique are described. Commercial graphite powder (Sigma Aldrich, catalog number 808113) was used for the ink synthesis. The graphite was first exfoliated in ethanol, an inexpensive and environmentally benign solvent, with ethyl cellulose (EC) as surfactants which protects graphene flakes from agglomeration. An ultrasonic probe with maximum 500-watt power with 20kHz frequency was used for the process. Subsequently, a sedimentation-based centrifugation and flocculation based on the addition of sodium chloride were employed to remove remaining large graphite flakes and excess EC, respectively. The resulting graphene/EC solid was subsequently washed and dried, yielding a black powder. The conductive graphene ink was synthesized by dispersing graphene/EC powder in a cyclohexanone/terpineol mixture. The detailed process is as follows:

Step 1. Ethyl cellulose was completely dispersed in ethanol with bath sonication followed by mixing of pristine graphite flakes ( $20 \text{ mg ml}^{-1}$ ).

Step 2. Probe sonication was used to exfoliate graphite with an ice bath to avoid the rise in the temperature that has detrimental effects.

Step 3. The graphene/EC dispersion was then centrifuged at 10000g (equivalent to 11641rpm) for 15 minutes to remove remaining large graphite flakes from the mixture.

Step 4. After centrifugation, 40 mg ml<sup>-1</sup> sodium chloride solution was added in the graphene/EC supernatant with a volume ratio of 1:2, followed by few minutes of stirring. This flocculation process results in the removal of excess ethyl cellulose. The graphene/EC composite was then isolated by vacuum filter and washed with deionized water to remove the residual salt.

Step 5. The dried graphene/EC powder was re-dispersed in ethanol and filtered through 5µm filter to remove any remaining large size agglomeration.

Step 6. The material obtained in step 5 flocculated again with 40 mg ml<sup>-1</sup> sodium chloride solution.

Step 7. The collected dry graphene/EC powder was dispersed in cyclohexanone/terpineol mixture with a volume of ratio 85:15 at a concentration of 100 mg ml<sup>-1</sup>.

The graphene ink thus synthesized remains stable for months without agglomeration or sedimentation. Note that we have used a cyclohexanone and terpineol mixture as our solvent medium to suspend the active particles. Aqueous based solvents have been used by some researchers recently, however, due to their relatively high surface tension special precautions are taken. Other commonly used organic solvents such as dimethylformamide and chloroform are also not ideal for use as solvent medium for exfoliation and suspension due to their high volatility and toxic nature. We used an economic and environment-benign solvent, ethanol, which has aliphatic chain in the hydrophobic region and hydroxyl groups in the hydrophilic region contributing to the dispersion of graphene. Ethyl cellulose has been established as a promising polymeric surfactant

for graphene dispersion that protects it from agglomeration and can be easily removed by annealing [85, 87, 91]. The ice bath in the second process step above aims to avoid a high temperature that might cause the agglomeration of exfoliated graphene during the process. In the fourth step, a room-temperature flocculation of graphene/EC was achieved based on adding inorganic salt. Upon the addition of sodium chloride, ethyl cellulose encapsulated graphene gets agglomerated with a stirring process that can be easily subsequently collected. The relatively small size graphene flakes are necessary for the stability of conductive graphene inks as well as printed devices (the large particles would potentially lead to the clogging of the inkjet print head and/or nozzle). To make this possible, a filtration was used in step 5 above. Finally, we use a cyclohexanone/terpineol solvent system with a volume ratio of 85:15 to produce graphene inks. The surface tension of both solvents is close to that of graphene, helping the particles well suspended in the solvent. It can also prevent the coffee ring phenomenon during printing. "Coffee ring" originates from the capillary flow induced by the differential evaporation rates across the drop, liquid evaporating from the edge is replenished by liquid from the interior [103]. To avoid this phenomenon, few approaches were followed such as adding surfactants to reduce the surface tension gradient in the solvent and thus to manipulate the motion of the solute particles (as in this work), and applying mixed solvent system, where one solvent has a higher boiling point and lower surface tension than the other solvent [104].

## **2.2 Optimization of graphene inks**

This section is aimed to investigate ideal synthesis conditions for the yielding of high concentration graphene inks by varying some of the key parameters involved. Specifically, the concentration of surfactants (C), sonication time (t) and sonication energy (E) used during the synthesis of the ink were examined. Ultraviolet–visible spectroscopy (UV-Vis) was performed on

the ink to optimize the dispersion, a technique often used to determine quantitatively the concentrations of an absorbing substance in a solution [105-106]. Since our inks are designed for printed electronics, eventually, the electrical resistances of the all the inks were tested and the resistance of the optimized ink was supported to the UV-Vis experimental finding.

### 2.2.1 Ultraviolet–visible spectroscopy (UV-Vis)

Ultraviolet–visible spectroscopy (UV-Vis) is a quantitative technique used to measure the wavelength dependent light absorption by the material. According to Beer–Lambert law where  $A$  is the measured absorbance,  $c$  the concentration of the absorbing species,  $\epsilon$  is a constant known as the molar absorptivity or extinction coefficient, and  $l$  is the path length of light through the sample,  $A = \epsilon c l$  [107], the concentration is proportional to absorbance. Optical absorption spectroscopy of liquid-phase exfoliation produced graphene suspensions with surfactants was extensively studied. Coleman's group reported the absorption coefficient at the wavelength of 660 nm for graphene in SDBS was calculated to be  $\langle\alpha_{660}\rangle = 1390 \text{ mL mg}^{-1} \text{ m}^{-1}$ . For N-Methyl-2-Pyrrolidone, Gamma-butyrolactone and other surfactants, an average absorption coefficient is  $\langle\alpha_{660}\rangle = 2460 \text{ mL mg}^{-1} \text{ m}^{-1}$  [108]. Other groups reported aqueous-based graphene solutions show extremely large variability of absorption coefficients, start from  $\langle\alpha_{660}\rangle = 710 \text{ mL mg}^{-1} \text{ m}^{-1}$  and reach up to  $\langle\alpha_{660}\rangle = 6600 \text{ mL mg}^{-1} \text{ m}^{-1}$  [109-110].

At first, graphite was exfoliated in ethanol with different concentrations of surfactants at a fixed sonication time and sonication power, 2h and 100% energy ( $E = 500$  watts) respectively. Figure 2.1 shows the UV-Vis absorption spectrum of the graphene inks with concentration ( $C$ ) values of  $5 \text{ mg ml}^{-1}$ ,  $10 \text{ mg ml}^{-1}$ ,  $15 \text{ mg ml}^{-1}$ , and  $20 \text{ mg ml}^{-1}$  ethyl cellulose, providing support for the ink synthesis conditions. The absorption curves are almost overlapping for graphene inks with  $15 \text{ mg ml}^{-1}$  and  $20 \text{ mg ml}^{-1}$  ethyl cellulose, however, graphene inks with  $5 \text{ mg ml}^{-1}$  and  $10 \text{ mg ml}^{-1}$

<sup>1</sup> ethyl cellulose have significantly different absorbance. The absorbance of graphene inks decreased notably with the increasing ethyl cellulose concentration. As the next step of optimization processes, therefore, remaining factors (sonication time and sonication energy) were varied keeping the ethyl cellulose concentration as 5 mg ml<sup>-1</sup> and 10 mg ml<sup>-1</sup>.

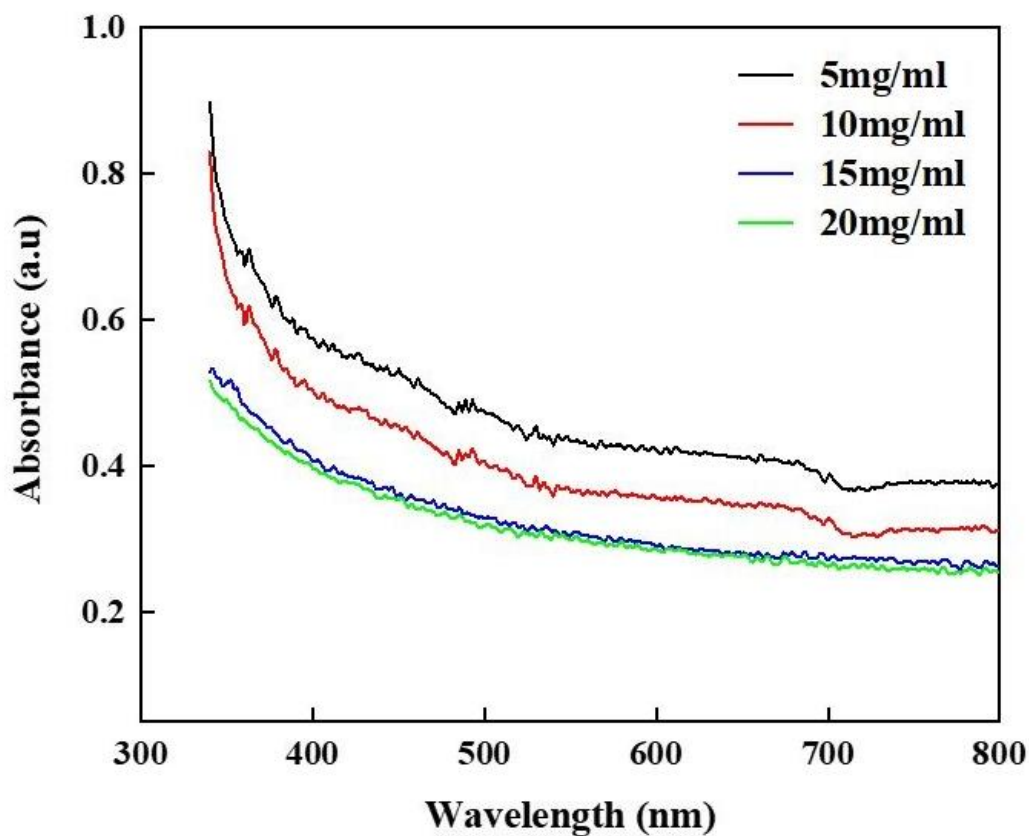
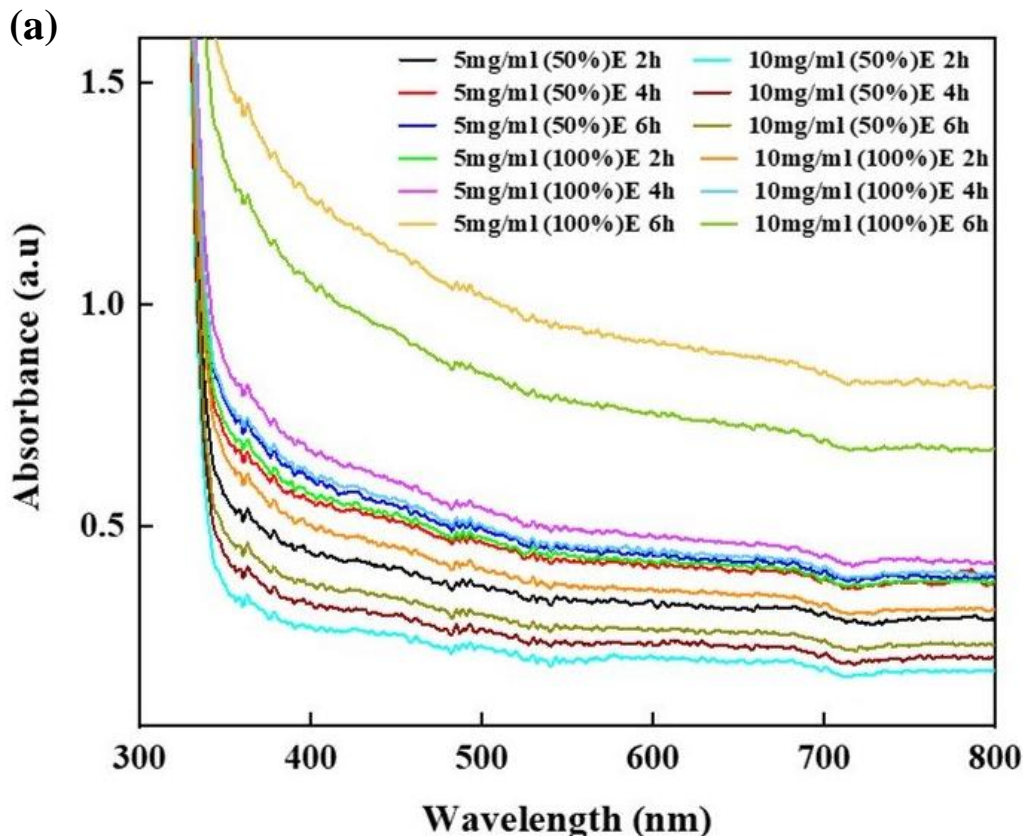


Figure 2.1. UV-Vis spectrum of graphene inks at different concentrations of ethyl cellulose with 2h sonication time and 100% sonication energy.

While longer sonication time and higher sonication energy may increase the concentration of the ink by more effective flake-surfactant conjugation, prolonged treatment and higher energy will also have risk of creating structural defects in graphene leading to detrimental properties.

Therefore, 12 batches of samples were prepared with three different variables - the concentration of ethyl cellulose ( $5 \text{ mg ml}^{-1}$  and  $10 \text{ mg ml}^{-1}$ ), sonication energy (50%E, and 100%E) and sonication time (2h, 4h, and 6h) and their absorption spectroscopy was studied.

Figure 2.2 below shows the original UV-Vis absorption spectra (a) and the scatter plot of graphene ink absorbance (b). The ink produced using  $5 \text{ mg ml}^{-1}$  ethyl cellulose has better performance than the one that uses  $10 \text{ mg ml}^{-1}$  (supporting earlier results). When we take the sonication energy into consideration, the higher sonication energy leads to superior results. When we consider inks obtained at different sonication time, the absorbance increased remarkably with the increasing sonication time at a constant sonication energy and ethyl cellulose concentration. It is evident from the figure that the graphene ink with  $5 \text{ mg ml}^{-1}$  ethyl cellulose, 6h sonication time and 100% sonication energy showed the highest absorbance.



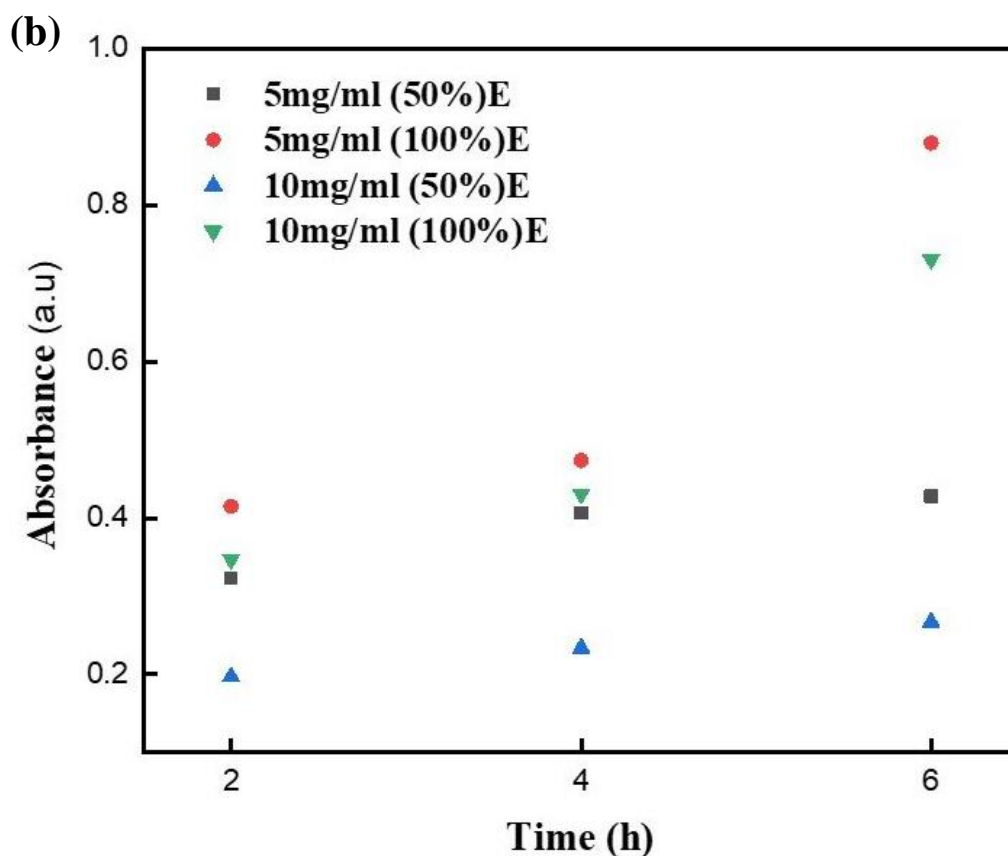


Figure 2.2. (a) the original UV-Vis absorption spectra and (b) the scatter plot of graphene ink absorbance of 12 batches of graphene inks with three variables- the concentration of ethyl cellulose ( $5 \text{ mg ml}^{-1}$  and  $10 \text{ mg ml}^{-1}$ ), sonication energy (50%E, and 100%E) and sonication time (2h, 4h, and 6h).

### 2.2.2 Electrical resistance measurements

To be used for printed electronics such as printed sensors, the graphene inks were first printed on various substrates followed by annealing in an inert environment and electrical resistance measurements were carried out using a digital multi-meter (DMM). Van der Paw geometry was used and the average resistance was measured. For a good comparison among above twelve inks, all of them were printed on polyimide substrates. Printed pattern with square geometry

with 5 mm x 5 mm area and 2 passes of printing for the resistance test is reported as the best values. Figure 2.3 shows the pictures of the synthesized inks and the printed patterns made from the inks. The printed patterns were first dried overnight at room temperature followed by annealing in a nitrogen environment at 350 °C for 2 hours duration. The annealing step was followed to remove surfactants and solvents from the material. For resistance measurements, the silver paste was applied to four corners of the square pattern for contacts and the resistance of graphene patterns was measured using a DMM.

Table 2.1 shows the electrical resistance of printed graphene patterns. The graphene ink that uses a surfactant (ethyl cellulose) concentration of 5 mg ml<sup>-1</sup> shows lower resistance value than those with 10 mg ml<sup>-1</sup> ethyl cellulose, especially under the long sonication time and high exfoliation energy. This is consistent with the results obtained from UV-Vis spectroscopy. Higher probe sonication energy and longer duration have a better performance. It is worth noting that there were very high resistance values (overload as seen in the DMM) for graphene inks with 10 mg ml<sup>-1</sup> ethyl cellulose and 50%E. It is evident from the table that graphene ink that uses 5 mg ml<sup>-1</sup> ethyl cellulose as the surfactant, probe sonicated for 6 hours of sonication time and with 100% sonication energy, shows the lowest resistance. These have been treated as the optimized ink parameters. Higher duration of sonication was not tried further.

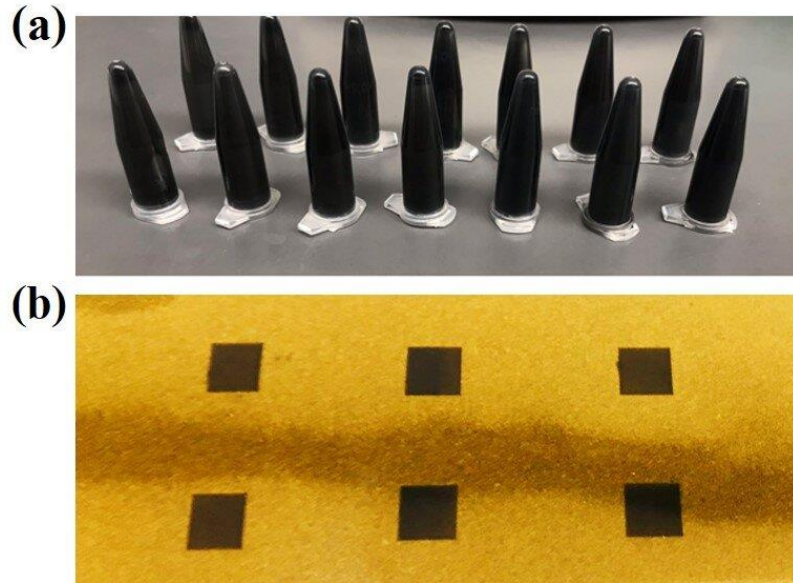


Figure 2.3. (a) Graphene inks with different EC concentration ( $\text{mg ml}^{-1}$ ), sonication energy (E) and sonication time (hr), (C, E, t): (5, 50%, 2), (5, 50%, 4), (5, 50%, 6), (5, 100%, 2), (5, 100%, 4), (5, 100%, 6), (10, 50%, 2), (10, 50%, 4), (10, 50%, 6), (10, 100%, 2), (10, 100%, 4), (10, 100%, 6), (15, 100%, 2), and (20, 100%, 2). (b) represented inkjet-printed graphene patterns with 5 mm x 5 mm area and two printing passes printed on polyimide substrates, with ink (5, 100%, 6).

Table 2.1. Resistance of printed graphene patterns.

|                                  |          | Sonication time        |                |                | Sonication time         |                |                |
|----------------------------------|----------|------------------------|----------------|----------------|-------------------------|----------------|----------------|
|                                  |          | 2h                     | 4h             | 6h             | 2h                      | 4h             | 6h             |
| Concentration of ethyl cellulose | 5 mg/ml  | 106.6K $\Omega$        | 97.7K $\Omega$ | 95.6K $\Omega$ | 96.5K $\Omega$          | 86.2K $\Omega$ | 17.7K $\Omega$ |
|                                  | 10 mg/ml | N/A                    | N/A            | N/A            | 105.2K $\Omega$         | 95.3K $\Omega$ | 43.8K $\Omega$ |
|                                  |          | Sonication energy 50%E |                |                | Sonication energy 100%E |                |                |

### 2.2.3 Dynamic light scattering (DLS)

The particle size of nanomaterials is important to investigate as their physical properties and chemical properties are very much dependent on the particle size. In case of graphene ink, it is also important for the quality of ink as well as the quality (including stability) of printed patterns. Dynamic light scattering (DLS) is one of the most versatile and useful techniques for characterizing the average size and size distribution of nanoparticles in a liquid [111]. It utilizes the illumination of particles or molecules in a solution undergoing Brownian motion by a laser beam. By analyzing the time-dependent fluctuations in the intensity of scattered light, the autocorrelation function of the signal can be determined [112]. Rapid and non-invasiveness of probing the particle size are significant advantages of the DLS method, however, it is worth noting that low particle concentration is necessary in this measurement to avoid particle-particle interactions in the dispersion.

In this study, a laser operating at a wavelength of 532 nm with a digital correlator from ALV500 (Software included) was used to measure the correlation function and hydrodynamic radius. A UV Quartz cuvette (light path: 10\*4mm) worked as a holder for liquid samples during the measurement. All measurements were taken at a room temperature of 25 °C. Each of the above samples was diluted 100 times and light scattering experiments were taken at least three times to for the accuracy and repeatability. The average diameters of graphene/EC composites in inks are summarized in Table 2.2. The particle size varies from 380 nm to 510 nm. The particle radius of the best performance graphene ink according to UV-Vis and resistance measurement is 446 nm.

Table 2.2. Particle size of graphene/EC particles in inks.

|                                  |          | Sonication time        |       |       | Sonication time         |       |       |
|----------------------------------|----------|------------------------|-------|-------|-------------------------|-------|-------|
|                                  |          | 2h                     | 4h    | 6h    | 2h                      | 4h    | 6h    |
| Concentration of ethyl cellulose | 5 mg/ml  | 430nm                  | 425nm | 460nm | 380nm                   | 480nm | 446nm |
|                                  | 10 mg/ml | 500nm                  | 510nm | 338nm | 407nm                   | 490nm | 420nm |
|                                  |          | Sonication energy 50%E |       |       | Sonication energy 100%E |       |       |

## Chapter 3 – Electrochemical properties

The goal of the present chapter is to describe the development of a hybrid or composite graphene inks for printed electronics. The materials presented in this chapter constitute part of a non-provisional PCT application (Kansas State University Disclosure Number 2019-066), filed on June 25, 2020, as follows.

*“Nano-inks of Carbon Nanomaterials for Printing and Coating, PCT Application No.: PCT/US2020/039547”*

In the present chapter, the electrochemical performance of the optimized graphene ink was studied. Also, graphene-based hybrid inks were formulated by adding graphene aerosol gel and multi-walled carbon nanotubes, respectively. For comparison, we utilized a commercial graphene ink as the substitute for the synthesized graphene ink and performed similar hybrid inks and tested their electrochemical properties. Inkjet printing technique was applied to fabricate flexible electrochemical sensors. Cyclic voltammetry method was used to study the electrochemical properties.

### 3.1 Graphene and hybrid graphene conductive inks

Graphene possesses a wide range of unique physical properties, such as large surface areas, high thermal conductivity, high electron mobility, excellent mechanical stability, and chemical durability, which makes graphene very attractive for various types of sensing applications including, optical sensors, electric field sensors as well as electrochemical and biochemical sensors [1]. To further improve the performance of graphene sensing applications, carbon nanomaterials including carbon nanotubes, carbon nanofibers, and carbon black have been used as additive materials, where graphene acts as the matrix element and the secondary additive is used in a controlled concentration [113]. In this chapter, printable graphene derivative inks were formulated

by adding graphene aerosol gel (GAGs) and multi-walled carbon nanotubes (MWCNTs) into optimized graphene ink, respectively. Alternatively, they are called hybrid graphene inks. Hybrid inks from the commercial graphene ink added with GAGs and MWCNTs were also developed for comparison.

Graphene aerosol gel was obtained by gas-phase hydrocarbon ( $C_2H_2$ ) detonation with oxygen ( $O_2$ ). The catalyst-free controlled detonation of  $C_2H_2$  gas in the presence of  $O_2$  took place in a closed chamber where the hydrocarbon was first converted into free carbon atoms or ions and then condensed into a nanoparticle carbon aerosol. The nanometer-sized carbon eventually bonded together forming a gel-like morphology [114]. Nanotubes are chemically inert by nature. Assuming no defected structure and the edge-states at both ends are passivated. Single-walled carbon nanotubes have therefore attracted much attention in high-capacity storage devices due to the extraordinary large irreversible capacities, while tend to aggregate into bundles because of relatively high surface energy and large aspect ratio. Multi-walled carbon nanotubes are more generally used in oxygen reduction reactions (ORR), such as fuel cells, due to superior thermal and chemical stability. Further, the price-friendliness of multi-walled carbon nanotubes also facilitates practical applicability [115].

The optimized in-house graphene ink was produced by liquid-phase exfoliation in ethanol, with  $5 \text{ mg ml}^{-1}$  ethyl cellulose, 6h of sonication time, and 100% sonication energy. Also, a known commercial graphene ink was purchased from Sigma-Aldrich containing 2.4 wt. % graphene/ethyl cellulose solid in an 85:15 cyclohexanone/terpineol mixture. Multi-walled carbon nanotubes were purchased from NanoIntegris with an out-layer diameter of less than 20 nm. Graphene aerosol gel was obtained by gas-phase hydrocarbon ( $C_2H_2$ ) detonation with oxygen ( $O_2$ ), the pre-detonation molar ratio of  $O_2/C_2H_2$  is 0.5. Graphene aerosol gels and multi-walled carbon nanotubes were

dispersed in pure graphene ink respectively with a concentration of  $0.3 \text{ mg ml}^{-1}$ . An hour bath sonication for the dispersion was employed to obtain uniform graphene-based composite ink that was suitable for inkjet printing.

### **3.2 Fabrication of electrodes**

Printing technology is evolving as a promising method for the scalable production of devices at low cost and minimal waste of the materials, compared with traditional methods such as electroplating and etching processes, it avoids the complex processing steps and the use of toxic chemicals. To date, among various printing methods established based on liquid phase exfoliated ink processing, inkjet printing has shown outstanding performance in terms of the high spatial resolution with complex geometrical patterns. The surface tension and viscosity of the inks are crucial parameters [56].

Here, electrochemical sensors were patterned on flexible polyimide substrates (purchased from 3M) via the Inkjet printer (SonoPlot, Microplotter II, USA). Substrates were thoroughly cleaned with acetone, methanol, and deionized water with bath sonication and dried by the flowing nitrogen gas before use. Graphene ink was filled in a glass pipette with a tip with 20-micron diameter which was attached with the piezoelectric dispenser of the micro-plotter. The printed patterns were first dried at room temperature followed by 2 hours of annealing at  $350 \text{ }^\circ\text{C}$  in  $\text{N}_2/\text{H}_2$  mixture (5% hydrogen in nitrogen). This process burns off surfactants and solvents. Ethyl cellulose decomposition generally occurs in two stages, a low-temperature charring beginning below  $250 \text{ }^\circ\text{C}$  and the total removal of the residue occurring at temperatures above  $400 \text{ }^\circ\text{C}$ . The decomposition of EC at the temperature of  $250\text{--}350 \text{ }^\circ\text{C}$  enables efficient charge transport through the graphene network because cellulose derivatives can thermally decompose into aromatic species resulting in  $\pi\text{--}\pi$  stacking between the residues and the graphene flakes [116].

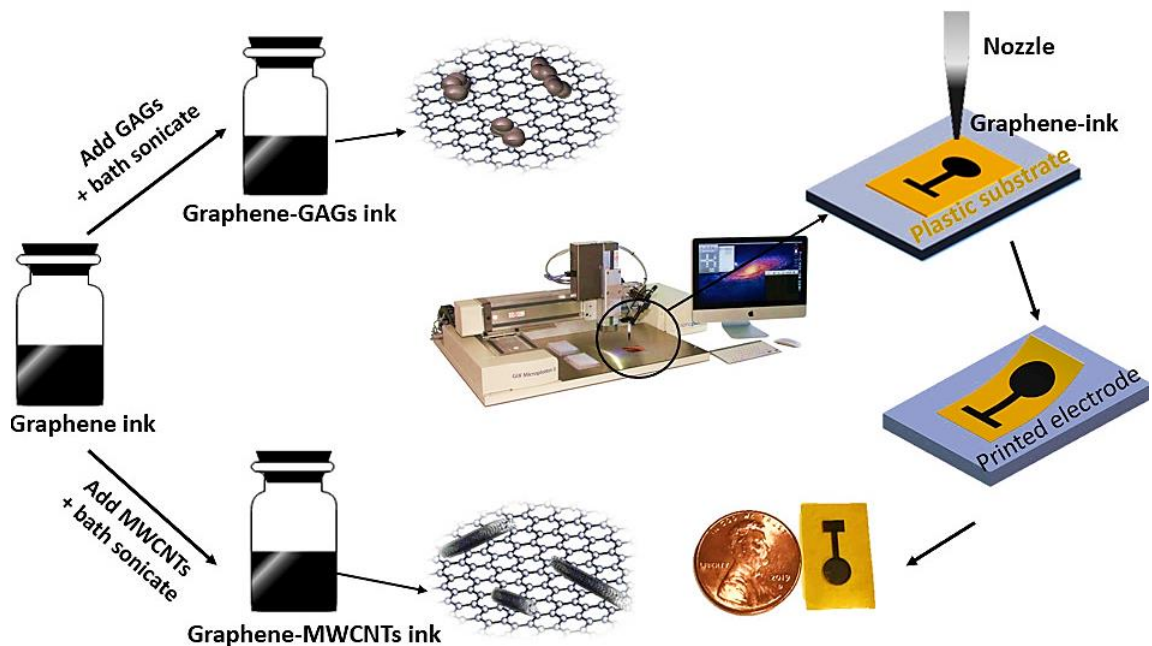


Figure 3.1. Schematic of graphene composite ink fabrication and inkjet printing process.

### 3.3 Cyclic voltammetry (CV)

Cyclic voltammetry (CV) is a very versatile electrochemical technique that can be used to acquire qualitative and quantitative information about electrochemical reactions, including the reversibility of reactions, reaction mechanisms, electrochemical kinetics, electrocatalytic processes, and others [117]. Here, CV was applied to investigate the electrochemical behavior of pure graphene, graphene-GAGs and graphene-MWCNTs inks. A traditional three-electrode-cell system was used for the CV measurement where a silver/silver chloride (Ag/AgCl) electrode worked as the reference electrode, a platinum wire and the inkjet-printed electrode served as the counter electrode and working electrode, respectively. As a simple outer-sphere redox couple, hexaammineruthenium(III) chloride  $[\text{Ru}(\text{NH}_3)_6]^{2+/3+}$  is relatively insensitive to the surface

microstructure and surface oxides leading to a faster and more reversible reaction [118]. Therefore, CV measurements were carried out with the hexaammineruthenium(III) chloride solution containing potassium chloride. All the CV measurements were repeated three times.

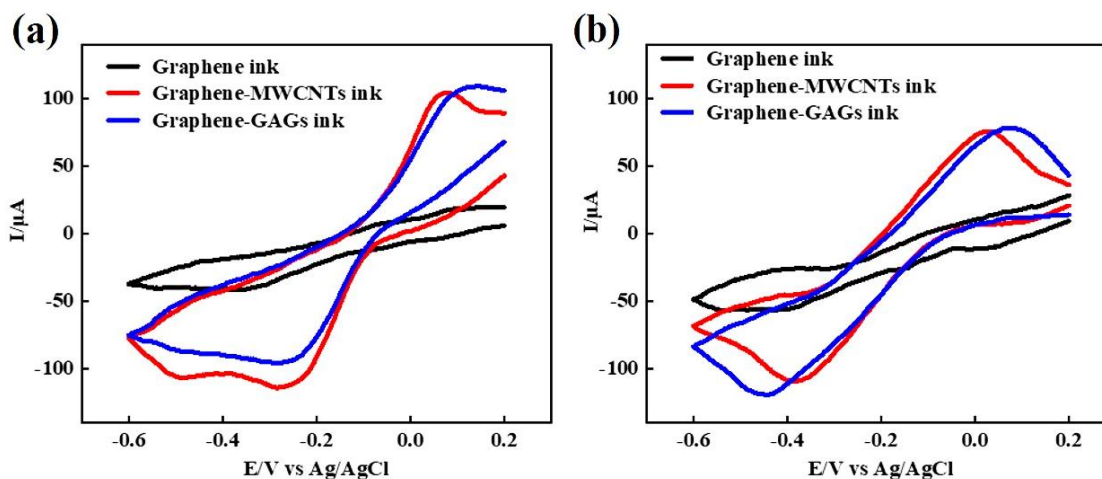


Figure 3.2. Cyclic voltammograms of graphene (black), graphene-GAGs (blue) and graphene-MWCNTs (red) sensors based on (a) the synthesized graphene ink and (b) a commercial graphene ink in 5.0mM  $[\text{Ru}(\text{NH}_3)_6]^{2+/3+}$  containing 0.1M KCl at the scan rate of  $100 \text{ mV s}^{-1}$ .

Figure 3.2(a) shows the CV curves of pure graphene, graphene-GAGs, and graphene-MWCNTs electrodes at a sweep rate ( $V$ ) of  $100 \text{ mV s}^{-1}$  in the  $5.0 \text{ mM } [\text{Ru}(\text{NH}_3)_6]^{2+/3+}$  solution containing  $0.1\text{M KCl}$ . The bare graphene electrode shows ignorable redox current peaks under the potential range between  $0.2$  and  $-0.6\text{V}$  indicating a low sensitivity. On the contrary, either graphene- GAGs or graphene-MWCNTs electrode shows a pair of well-defined redox peaks with  $I_{pa}/I_{pc} \approx 1$  vs.  $[\text{Ru}(\text{NH}_3)_6]^{2+/3+}$ . The substantial increase of electrochemical currents is direct evidence of the enhanced charge transfer rate in composite electrodes. Further, the smaller redox potential separation on graphene-MWCNTs electrodes, calculated by equation  $\Delta E_p = E_{pa} - E_{pc}$ ,

pointing out that the reversibility was further improved by the presence of the multi-walled carbon nanotubes. The shift of the electrochemical potential might be due to the concentration polarization resulting from the different rate of electrochemical reaction at the electrode surface and the ion migration to the electrode surface.

For comparison, the only known commercial graphene ink for inkjet printing was used to replace the synthesized graphene ink for the manufacture of hybrid inks and electrodes. As shown in Figure 3.2(b), electrochemical behaviors are consistent with that of the synthesized graphene inks. The addition of graphene aerosol gels and multi-walled carbon nanotubes, as seen from two different graphene inks, led to a better electrochemical performance reflecting on the increase of redox currents. Among the three inks, graphene-MWCNTs electrode has the most outstanding electrochemical properties. While the use of synthesized graphene ink as a matrix well compared with a commercial graphene ink in terms of the magnitude of redox peak currents and the separation between the peak potentials, further improvements are still needed for further enhancement of electrochemical activities.

The effect of scan rates on the redox reaction at graphene-GAGs and graphene-MWCNTs electrodes based on synthesized graphene inks was studied. As shown in Figure 3.3, the magnitude of anodic ( $I_{Pa}$ ) and cathodic ( $I_{Pc}$ ) peak currents rise with the increase of scan rate ranging from 5 to 100  $\text{mV s}^{-1}$ , and show a good linear relationship with the square root of scan rates ( $V^{1/2}$ ), indicating that the reaction is controlled by the diffusion process. However, the peak-to-peak separation becomes larger and the ratio of the anodic peak current to the cathodic peak current is also different from unity. The linear regression equations of graphene-GAGs electrodes (Figure 18(b)) are expressed as  $I_{Pa} = 17.514 + 5.399x$  ( $R^2 = 0.9746$ ) and  $I_{Pc} = -12.645 - 4.494x$  ( $R^2 = 0.9827$ ). Similarly, Figure 18(d) shows linear regression equations of graphene-MWCNTs

electrodes as  $I_{pa} = -3.645 + 7.586x$  ( $R^2 = 0.9947$ ) and  $I_{pc} = -12.104 - 6.2638x$  ( $R^2 = 0.9902$ ).  $R^2$  is the correlation of determination showing the linear effect of the square root of scan rates on the peak current. The results provide further evidence that the addition of graphene aerogels and multi-walled carbon nanotubes endows fast electron transfer.

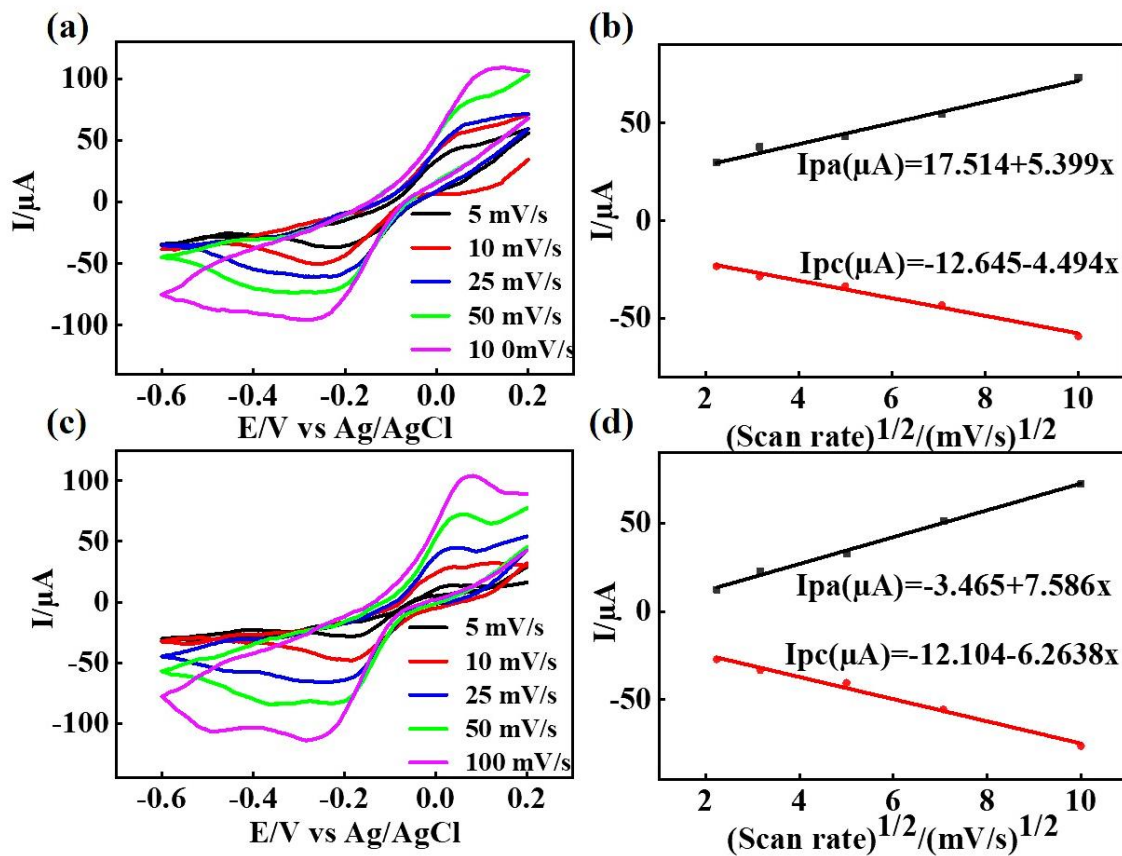


Figure 3.3. Cyclic voltammograms of synthesized graphene ink-based graphene-GAGs electrode (a) and graphene-MWCNTs electrode (c) in 5.0mM  $[\text{Ru}(\text{NH}_3)_6]^{2+/3+}$  in 0.1M KCl with scan rates: 5, 10, 25, 50 and 100  $\text{mV s}^{-1}$ . The dependence of the peak current at graphene-GAGs electrode (b) and graphene-MWCNTs electrode (d) on the square root of scan rates.

Figure 3.4 shows the peak currents of commercial graphene ink-based graphene-GAGs electrodes and graphene-MWCNTs electrodes, also varies in a linear relation with  $V^{1/2}$  that from 5 to 100  $\text{mV s}^{-1}$ . The linear regression equations of graphene-CAGs electrodes (Figure 19(b)) and graphene-MWCNTs electrodes (Figure 19(d)) are expressed as  $I_{pa} = 10.933 + 7.965x$  ( $R^2 = 0.9721$ );  $I_{pc} = -1.882 - 9.452x$  ( $R^2 = 0.9901$ ) and  $I_{pa} = 16.4026 + 7.632x$  ( $R^2 = 0.9792$ );  $I_{pc} = -1.2953 - 9.4544x$  ( $R^2 = 0.9961$ ), respectively. The synthesized graphene ink-based electrodes show identical trend and comparable performance with the commercial graphene ink-based electrodes. However, it is worth noting that the larger slope of commercial inks indicating a better mass transfer effect. Future potential improvements remain open for more research in this field.

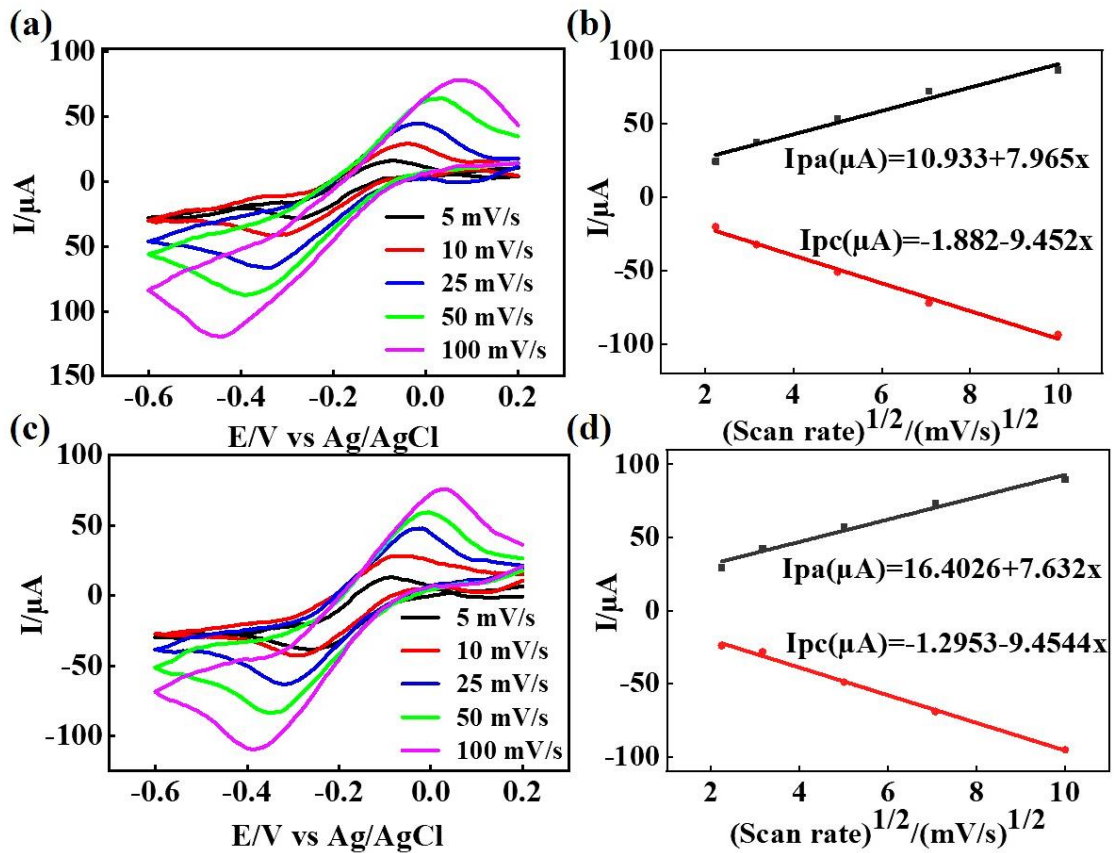


Figure 3.4. Cyclic voltammograms of commercial graphene ink-based graphene-GAGs electrode (a) and graphene-MWCNTs electrode (c) in 5.0mM  $[\text{Ru}(\text{NH}_3)_6]^{2+/3+}$  in 0.1M KCl with scan rates: 5, 10, 25, 50 and 100  $\text{mV s}^{-1}$ . The dependence of the peak current at graphene-GAGs electrode (b) and graphene-MWCNTs electrode (d) on the square root of scan rates.

Further, from the linear fitting of the Randles-Sevcik equation [119]:

$$I_p = (2.69 \times 10^5)n^{3/2}AD^{1/2}CV^{1/2}$$

Where A is the effective surface area ( $\text{cm}^2$ ),  $I_p$  is the peak current of the redox reaction,  $n$  is the number of electrons transferred during the electrochemical process ( $n=1$ ), D is the diffusion coefficient ( $6.0 \times 10^{-6} \text{ cm}^2 \text{ s}^{-1}$  for  $[\text{Ru}(\text{NH}_3)_6]^{2+/3+}$ ), V is the scan rate ( $\text{V s}^{-1}$ ) and C is the concentration of  $[\text{Ru}(\text{NH}_3)_6]^{2+/3+}$  ( $\text{mol L}^{-1}$ ). The peak currents shown in the figures above are lower than those theoretically calculated that might due to the real surface area of the working electrode not being entirely active.

## **Chapter 4 - Summary and outlook**

### **4.1 Summary of thesis research**

With the ever-demanding field of printed electronics, in conjunction with additive manufacturing and atomically thin carbon nanomaterials such as graphene, there is great demand for manufacturing of electrochemical sensors and electronic devices. New functionalities and cost-performance tradeoffs compared to traditional methods are primary driving factors. A major challenge of printed electronics is the development of diverse functional liquid-phase inks offering outstanding electrical and mechanical performance, suitable stability as well as rapid and effective printing. Graphene is an excellent material for a range of printed electronics applications based on the high surface area, great electrical conductivity, robust mechanical, chemical, and thermal stability. This thesis describes a compelling platform for graphene ink development for integration in printed devices. By using the liquid-phase exfoliation technique with a cellulosic polymer as multifunctional surfactants, a combination of simplified processes, stable ink formulation, and competitive ink performance is realized. To further improve the performance of graphene sensing applications, graphene aerosol gel (GAGs) and multi-walled carbon nanotubes (MWCNTs) were introduced into optimized graphene ink. For comparison, we utilized a commercial graphene ink as the substitute for the synthesized graphene ink and conducted the corresponding experiments. Inkjet printer serves as a tool for the fabrication of devices.

Chapter 1 outlines the necessary background of graphene, the motivation and synthesis of graphene-based conductive inks, and the recent progress of graphene-based conductive inks.

Chapter 2 outlines the processing framework and the optimization for graphene inks. This chapter details the general experimental procedure for the development of graphene inks based on exfoliation, centrifugation, and flocculation. It also investigates ideal synthesis conditions for the

yielding of high concentration graphene inks, providing important context for the subsequent work. Specifically, the concentration of surfactants (5 mg ml<sup>-1</sup>, 10 mg ml<sup>-1</sup>, 15 mg ml<sup>-1</sup>, and 20 mg ml<sup>-1</sup>), sonication time (2h, 4h, and 6h), and sonication energy (50%E and 100%E) were studied. Ultraviolet–visible spectroscopy (UV-Vis) was performed on the ink for optimization, a technique often used to determine quantitatively concentrations of an absorbing substance in a solution. The absorbance of graphene inks decreased notably with the increasing ethyl cellulose concentration. Longer sonication time and higher sonication energy increase the concentration of the ink by more effective flake-surfactant conjugation. Higher duration of sonication was not tried further since prolonged treatment and higher energy will have also risk of creating structural defects in graphene leading to detrimental properties. Electrical resistance was measured via a Van der Pauw geometry and a digital multi-meter (DMM). Printed graphene patterns, with 5 mm x 5 mm area and 2 passes of printing, were annealed in a nitrogen environment at 350 °C for 2 hours duration to remove surfactants and solvents from the material. The graphene ink that uses a lower surfactant concentration shows smaller resistance value, especially under the long sonication time and high exfoliation energy. The results are consistent with the UV-Vis spectroscopy. The average diameter of graphene/EC composites in inks is characterized by dynamic light scattering (DLS). The particle radius varies from 380 nm to 510 nm. Therefore, 5 mg ml<sup>-1</sup> ethyl cellulose concentration, 6h sonication time, and 100% sonication energy (500-watts) are the best combination so far.

Chapter 3 extends the graphene ink formulation framework by adding graphene aerosol gel and multi-walled carbon nanotubes. Inkjet printing technique was applied to fabricate flexible electrochemical redox sensors. Cyclic voltammetry (CV) served as a detection technique. For further comparison, a commercial graphene ink was used as the substitute for the synthesized graphene ink for corresponding experiments. Electrochemical sensors were patterned on flexible

polyimide substrates (purchased from 3M) via the Inkjet printer. CV measurements were performed under a traditional three electrodes system and a hexaammineruthenium(III) chloride solution containing potassium chloride. The bare graphene electrode shows ignorable redox current peaks indicating a low sensitivity. In contrast, either graphene-GAGs or graphene-MWCNTs electrode shows a pair of well-defined redox peaks with  $I_{Pa}/I_{Pc} \approx 1$ . However, the smaller redox potential separation on graphene-MWCNTs electrodes pointing out that the reversibility was further improvised by the presence of the multi-walled carbon nanotubes. Electrochemical behaviors of commercial graphene ink-based sensors are consistent with that of the synthesized graphene ink. The addition of graphene aerosol gels and carbon nanotubes does lead to better electrochemical performance reflected in the increase of redox currents, among which the graphene-MWCNTs electrode has the most outstanding electrochemical properties. From the study of the effect of scan rates on the redox reactions at graphene-GAGs and graphene-MWCNTs electrodes, the magnitude of current peaks is proportional to the square root of scan rates ( $V^{1/2}$ ), indicating that the reaction is controlled by the diffusion process. The linear regression equations providing further evidence that the addition of graphene aerogels and carbon nanotubes endows fast electron transfer. The commercial graphene ink-based electrodes show an identical trend with synthesized graphene ink-based electrodes. While the use of synthesized graphene ink as a matrix well compared with a commercial graphene ink, future potential improvements remain open for more research in this field due to the more symmetrical redox peaks and larger slope of linear regression equations of commercial graphene-based electrodes.

## 4.2 Outlook

This research exhibits reasonable potential for graphene-based inks in practical electrochemical sensors. Number of potential applications of the technology could be explored,

the most immediate ones being the glucose sensors. Diabetes has become a global threat to human health that is seriously affecting millions of people. Advanced enzymatic glucose sensors have been extensively used due to the relatively high sensitivity and selectivity; however, the broad application is restricted by the intrinsic nature of the enzymes including too sensitive to environmental factors such as temperature and PH value, complicated immobilization process, low stability, and relatively high cost [120]. Therefore, the enzyme-free glucose sensor that frees from the drawbacks mentioned above is more attractive and feasible. Among a wide variety of nanomaterials that have been applied to the high response glucose sensors over the past decades, graphene shows an eye-catching performance. Our graphene-based inks could be competitive in the manufacture of enzyme-free printed glucose sensors.

## References

- [1] Novoselov, K. S., Geim, A. K., Morozov, S. V., Jiang, D., Zhang, Y., Dubonos, S. V., ... Firsov, A. A. (2004). Electric field effect in atomically thin carbon films. *Science*, 306(5696), 666–669.
- [2] Wallace, P. R. (1947). The band theory of graphite. *Physical Review*, 71(9), 622.
- [3] Ohashi, Y., Koizumi, T., Yoshikawa, T., Hironaka, T., & Shiiki, K. (1997). Size effect in the in-plane electrical resistivity of very thin graphite crystals. *Tanso*, 1997(180), 235–238.
- [4] Shams, S. S., Zhang, R., & Zhu, J. (2015). Graphene synthesis: a Review. *Materials Science-Poland*, 33(3), 566–578.
- [5] Lee, C., Wei, X., Kysar, J. W., & Hone, J. (2008). Measurement of the elastic properties and intrinsic strength of monolayer graphene. *Science*, 321(5887), 385–388.
- [6] Yang, G., Li, L., Lee, W. B., & Ng, M. C. (2018). Structure of graphene and its disorders: a review. *Science and Technology of Advanced Materials*, 19(1), 613–648.
- [7] Nourbakhsh, A., Cantoro, M., Klekachev, A. V., Pourtois, G., Vosch, T., Hofkens, J., ... Sels, B. F. (2011). Single layer vs bilayer graphene: a comparative study of the effects of oxygen plasma treatment on their electronic and optical properties. *The Journal of Physical Chemistry C*, 115(33), 16619–16624.
- [8] Balandin, A. A., Ghosh, S., Bao, W., Calizo, I., Teweldebrhan, D., Miao, F., & Lau, C. N. (2008). Superior thermal conductivity of single-layer graphene. *Nano Letters*, 8(3), 902–907.
- [9] McCann, E., & Fal'ko, V. I. (2006). Landau-level degeneracy and quantum Hall effect in a graphite bilayer. *Physical Review Letters*, 96(8), 86805.
- [10] Cançado, L. G., Reina, A., Kong, J., & Dresselhaus, M. S. (2008). Geometrical approach for the study of G' band in the Raman spectrum of monolayer graphene, bilayer graphene, and bulk graphite. *Physical Review B*, 77(24), 245408.
- [11] Craciun, M. F., Russo, S., Yamamoto, M., Oostinga, J. B., Morpurgo, A. F., & Tarucha, S. (2009). Trilayer graphene is a semimetal with a gate-tunable band overlap. *Nature Nanotechnology*, 4(6), 383–388.
- [12] Grüneis, A., Attaccalite, C., Wirtz, L., Shiozawa, H., Saito, R., Pichler, T., & Rubio, A. (2008). Tight-binding description of the quasiparticle dispersion of graphite and few-layer graphene. *Physical Review B*, 78(20), 205425.
- [13] Hao, Y., Wang, Y., Wang, L., Ni, Z., Wang, Z., Wang, R., ... Thong, J. T. L. (2010). Probing layer number and stacking order of few-layer graphene by Raman spectroscopy. *Small*, 6(2), 195–200.

- [14] Yu, V., & Hilke, M. (2009). Large contrast enhancement of graphene monolayers by angle detection. *Applied Physics Letters*, 95(15), 151904.[7]
- [15] Meyer, J. C., Geim, A. K., Katsnelson, M. I., Novoselov, K. S., Booth, T. J., & Roth, S. (2007). The structure of suspended graphene sheets. *Nature*, 446(7131), 60–63.
- [16] Das, A., Pisana, S., Chakraborty, B., Piscanec, S., Saha, S. K., Waghmare, U. V., ... Ferrari, A. C. (2008). Monitoring dopants by Raman scattering in an electrochemically top-gated graphene transistor. *Nature Nanotechnology*, 3(4), 210–215.
- [17] Ni, Z., Wang, Y., Yu, T., & Shen, Z. (2008). Raman spectroscopy and imaging of graphene. *Nano Research*, 1(4), 273–291.
- [18] Pimenta, M. A., Dresselhaus, G., Dresselhaus, M. S., Cancado, L. G., Jorio, A., & Saito, R. (2007). Studying disorder in graphite-based systems by Raman spectroscopy. *Physical Chemistry Chemical Physics*, 9(11), 1276–1290.
- [19] Wang, Y. Y., Ni, Z. H., Yu, T., Shen, Z. X., Wang, H. M., Wu, Y. H., ... Shen Wee, A. T. (2008). Raman studies of monolayer graphene: the substrate effect. *The Journal of Physical Chemistry C*, 112(29), 10637–10640.
- [20] Wu, J.-B., Lin, M.-L., Cong, X., Liu, H.-N., & Tan, P.-H. (2018). Raman spectroscopy of graphene-based materials and its applications in related devices. *Chemical Society Reviews*, 47(5), 1822–1873.
- [21] Stauber, T., Peres, N. M. R., & Geim, A. K. (2008). Optical conductivity of graphene in the visible region of the spectrum. *Physical Review B*, 78(8), 85432.
- [22] Geim, A. K. (2009). Graphene: status and prospects. *Science*, 324(5934), 1530–1534.
- [23] Meyer, J. C., Geim, A. K., Katsnelson, M. I., Novoselov, K. S., Booth, T. J., & Roth, S. (2007). The structure of suspended graphene sheets. *Nature*, 446(7131), 60–63.
- [24] Hass, J., De Heer, W. A., & Conrad, E. H. (2008). The growth and morphology of epitaxial multilayer graphene. *Journal of Physics: Condensed Matter*, 20(32), 323202.
- [25] Berger, C., Song, Z., Li, T., Li, X., Ogbazghi, A. Y., Feng, R., ... First, P. N. (2004). Ultrathin epitaxial graphite: 2D electron gas properties and a route toward graphene-based nanoelectronics. *The Journal of Physical Chemistry B*, 108(52), 19912–19916.
- [26] Edwards, R. S., & Coleman, K. S. (2013). Graphene synthesis: relationship to applications. *Nanoscale*, 5(1), 38–51.
- [27] Ohta, T., Bostwick, A., McChesney, J. L., Seyller, T., Horn, K., & Rotenberg, E. (2007). Interlayer interaction and electronic screening in multilayer graphene investigated with angle-resolved photoemission spectroscopy. *Physical Review Letters*, 98(20), 206802.

- [28] Choi, W., Lahiri, I., Seelaboyina, R., & Kang, Y. S. (2010). Synthesis of graphene and its applications: a review. *Critical Reviews in Solid State and Materials Sciences*, 35(1), 52–71.
- [29] Morozov, S. V, Novoselov, K. S., Katsnelson, M. I., Schedin, F., Ponomarenko, L. A., Jiang, D., & Geim, A. K. (2006). Strong suppression of weak localization in graphene. *Physical Review Letters*, 97(1), 16801.
- [30] Escobedo-Cousin, E., Vassilevski, K., Hopf, T., Wright, N., O’Neill, A., Horsfall, A., ... Cumpson, P. (2013). Local solid phase growth of few-layer graphene on silicon carbide from nickel silicide supersaturated with carbon. *Journal of Applied Physics*, 113(11), 114309.
- [31] Hofmann, S., Braeuninger-Weimer, P., & Weatherup, R. S. (2015). CVD-enabled graphene manufacture and technology. *The Journal of Physical Chemistry Letters*, 6(14), 2714–2721.
- [32] Li, X., Cai, W., An, J., Kim, S., Nah, J., Yang, D., ... Tutuc, E. (2009). Large-area synthesis of high-quality and uniform graphene films on copper foils. *Science*, 324(5932), 1312–1314.
- [33] Zhang, Y., Gomez, L., Ishikawa, F. N., Madaria, A., Ryu, K., Wang, C., ... Zhou, C. (2010). Comparison of graphene growth on single-crystalline and polycrystalline Ni by chemical vapor deposition. *The Journal of Physical Chemistry Letters*, 1(20), 3101–3107.
- [34] An, H., Lee, W.-J., & Jung, J. (2011). Graphene synthesis on Fe foil using thermal CVD. *Current Applied Physics*, 11(4), S81–S85.
- [35] Mohanty, N., & Berry, V. (2008). Graphene-based single-bacterium resolution biodevice and DNA transistor: interfacing graphene derivatives with nanoscale and microscale biocomponents. *Nano Letters*, 8(12), 4469–4476.
- [36] Ago, H., Ito, Y., Mizuta, N., Yoshida, K., Hu, B., Orofeo, C. M., ... Mizuno, S. (2010). Epitaxial chemical vapor deposition growth of single-layer graphene over cobalt film crystallized on sapphire. *ACS Nano*, 4(12), 7407–7414.
- [37] Ihm, K., Lim, J. T., Lee, K.-J., Kwon, J. W., Kang, T.-H., Chung, S., ... Yeom, G. Y. (2010). Number of graphene layers as a modulator of the open-circuit voltage of graphene-based solar cell. *Applied Physics Letters*, 97(3), 32113.
- [38] Wang, Y., Zheng, Y., Xu, X., Dubuisson, E., Bao, Q., Lu, J., & Loh, K. P. (2011). Electrochemical delamination of CVD-grown graphene film: toward the recyclable use of copper catalyst. *ACS Nano*, 5(12), 9927–9933.
- [39] Huss-Hansen, M. K., Hodas, M., Mrkyvkova, N., Hagara, J., Jensen, B. B. E., Osadnik, A., ... Schreiber, F. (2020). Surface-controlled crystal alignment of naphthyl end-capped oligothiophene on graphene: thin-film growth studied by in situ X-ray diffraction. *Langmuir*, 36(8), 1898–1906

- [40] Flint, E. B., & Suslick, K. S. (1991). The temperature of cavitation. *Science*, 253(5026), 1397–1399.
- [41] Han, J. T., Jang, J. I., Kim, H., Hwang, J. Y., Yoo, H. K., Woo, J. S., ... Jeong, S. Y. (2014). Extremely efficient liquid exfoliation and dispersion of layered materials by unusual acoustic cavitation. *Scientific Reports*, 4(1), 1–7.
- [42] Lotya, M., King, P. J., Khan, U., De, S., & Coleman, J. N. (2010). High-concentration, surfactant-stabilized graphene dispersions. *ACS Nano*, 4(6), 3155–3162.
- [43] Khan, U., O'Neill, A., Lotya, M., De, S., & Coleman, J. N. (2010). High-concentration solvent exfoliation of graphene. *Small*, 6(7), 864–871.
- [44] Zhu, Y., Murali, S., Cai, W., Li, X., Suk, J. W., Potts, J. R., & Ruoff, R. S. (2010). Graphene and graphene oxide: synthesis, properties, and applications. *Advanced Materials*, 22(35), 3906–3924.
- [45] Marcano, D. C., Kosynkin, D. V, Berlin, J. M., Sinitskii, A., Sun, Z., Slesarev, A., ... Tour, J. M. (2010). Improved synthesis of graphene oxide. *ACS Nano*, 4(8), 4806–4814.
- [46] Dreyer, D. R., Murali, S., Zhu, Y., Ruoff, R. S., & Bielawski, C. W. (2011). Reduction of graphite oxide using alcohols. *Journal of Materials Chemistry*, 21(10), 3443–3447.
- [47] Stankovich, S., Dikin, D. A., Piner, R. D., Kohlhaas, K. A., Kleinhammes, A., Jia, Y., ... Ruoff, R. S. (2007). Synthesis of graphene-based nanosheets via chemical reduction of exfoliated graphite oxide. *Carbon*, 45(7), 1558–1565.
- [48] Brumfiel, G. (2009). Nanotubes cut to ribbons new techniques open up carbon tubes to create ribbons. *Nature*.
- [49] Xie, L., Wang, H., Jin, C., Wang, X., Jiao, L., Suenaga, K., & Dai, H. (2011). Graphene nanoribbons from unzipped carbon nanotubes: atomic structures, Raman spectroscopy, and electrical properties. *Journal of the American Chemical Society*, 133(27), 10394–10397.
- [50] Jiao, L., Zhang, L., Wang, X., Diankov, G., & Dai, H. (2009). Narrow graphene nanoribbons from carbon nanotubes. *Nature*, 458(7240), 877–880.
- [51] Kosynkin, D. V, Higginbotham, A. L., Sinitskii, A., Lomeda, J. R., Dimiev, A., Price, B. K., & Tour, J. M. (2009). Longitudinal unzipping of carbon nanotubes to form graphene nanoribbons. *Nature*, 458(7240), 872–876.
- [52] Russo, A., Ahn, B. Y., Adams, J. J., Duoss, E. B., Bernhard, J. T., & Lewis, J. A. (2011). Pen-on-paper flexible electronics. *Advanced Materials*, 23(30), 3426–3430.
- [53] Karim, N., Afroj, S., Tan, S., Novoselov, K. S., & Yeates, S. G. (2019). All inkjet-printed graphene-silver composite ink on textiles for highly conductive wearable electronics applications. *Scientific Reports*, 9(1), 1–10.

- [54] Leng, T., Huang, X., Chang, K., Chen, J., Abdalla, M. A., & Hu, Z. (2016). Graphene nanoflakes printed flexible meandered-line dipole antenna on paper substrate for low-cost RFID and sensing applications. *IEEE Antennas and Wireless Propagation Letters*, *15*, 1565–1568.
- [55] Singh, M., Haverinen, H. M., Dhagat, P., & Jabbour, G. E. (2010). Inkjet printing—process and its applications. *Advanced Materials*, *22*(6), 673–685.
- [56] Inagaki, M., Konno, H., & Tanaike, O. (2010). Carbon materials for electrochemical capacitors. *Journal of Power Sources*, *195*(24), 7880–7903
- [57] Lee, H.-H., Chou, K.-S., & Huang, K.-C. (2005). Inkjet printing of nanosized silver colloids. *Nanotechnology*, *16*(10), 2436.
- [58] Deng, D., Jin, Y., Cheng, Y., Qi, T., & Xiao, F. (2013). Copper nanoparticles: aqueous phase synthesis and conductive films fabrication at low sintering temperature. *ACS Applied Materials & Interfaces*, *5*(9), 3839–3846.
- [59] Kim, Y., Lee, B., Yang, S., Byun, I., Jeong, I., & Cho, S. M. (2012). Use of copper ink for fabricating conductive electrodes and RFID antenna tags by screen printing. *Current Applied Physics*, *12*(2), 473–478.
- [60] Wakuda, D., Hatamura, M., & Suganuma, K. (2007). Novel method for room temperature sintering of Ag nanoparticle paste in air. *Chemical Physics Letters*, *441*(4–6), 305–308.
- [61] Hu, C.-C., Chang, K.-H., & Wang, C.-C. (2007). Two-step hydrothermal synthesis of Ru–Sn oxide composites for electrochemical supercapacitors. *Electrochimica Acta*, *52*(13), 4411–4418.
- [62] Sharma, P., & Bhatti, T. S. (2010). A review on electrochemical double-layer capacitors. *Energy Conversion and Management*, *51*(12), 2901–2912.
- [63] Novoselov, K. S., Fal, V. I., Colombo, L., Gellert, P. R., Schwab, M. G., & Kim, K. (2012). A roadmap for graphene. *Nature*, *490*(7419), 192–200.
- [64] Yang, G., Li, L., Lee, W. B., & Ng, M. C. (2018). Structure of graphene and its disorders: a review. *Science and Technology of Advanced Materials*, *19*(1), 613–648.
- [65] Raccichini, R., Varzi, A., Passerini, S., & Scrosati, B. (2015). The role of graphene for electrochemical energy storage. *Nature Materials*, *14*(3), 271–279.
- [66] Israelachvili, J. N. (2011). *Intermolecular and surface forces*. Academic press.
- [67] Brodie, B. C. (1859). XIII. On the atomic weight of graphite. *Philosophical Transactions of the Royal Society of London*, (149), 249–259.
- [68] Hummers Jr, W. S., & Offeman, R. E. (1958). Preparation of graphitic oxide. *Journal of the American Chemical Society*, *80*(6), 1339.

- [69] Marcano, D. C., Kosynkin, D. V., Berlin, J. M., Sinitskii, A., Sun, Z., Slesarev, A., ... Tour, J. M. (2010). Improved synthesis of graphene oxide. *ACS Nano*, 4(8), 4806–4814.
- [70] Park, S., An, J., Piner, R. D., Jung, I., Yang, D., Velamakanni, A., ... Ruoff, R. S. (2008). Aqueous suspension and characterization of chemically modified graphene sheets. *Chemistry of Materials*, 20(21), 6592–6594.
- [71] Pei, S., & Cheng, H.-M. (2012). The reduction of graphene oxide. *Carbon*, 50(9), 3210–3228.
- [72] Ciesielski, A., & Samori, P. (2014). Graphene via sonication assisted liquid-phase exfoliation. *Chemical Society Reviews*, 43(1), 381–398.
- [73] Narayan, R., & Kim, S. O. (2015). Surfactant mediated liquid phase exfoliation of graphene. *Nano Convergence*, 2(1), 1–19.
- [74] Israelachvili, J. N. (2011). *Intermolecular and surface forces*. Academic press.
- [75] Zacharia, R., Ulbricht, H., & Hertel, T. (2004). Interlayer cohesive energy of graphite from thermal desorption of polyaromatic hydrocarbons. *Physical Review B*, 69(15), 155406.
- [76] Lotya, M., Hernandez, Y., King, P. J., Smith, R. J., Nicolosi, V., Karlsson, L. S., ... McGovern, I. T. (2009). Liquid phase production of graphene by exfoliation of graphite in surfactant/water solutions. *Journal of the American Chemical Society*, 131(10), 3611–3620.
- [77] Fujigaya, T., & Nakashima, N. (2008). Methodology for homogeneous dispersion of single-walled carbon nanotubes by physical modification. *Polymer Journal*, 40(7), 577–589.
- [78] Dhakate, S. R., Chauhan, N., Sharma, S., Tawale, J., Singh, S., Sahare, P. D., & Mathur, R. B. (2011). An approach to produce single and double layer graphene from re-exfoliation of expanded graphite. *Carbon*, 49(6), 1946–1954.
- [79] Qian, W., Hao, R., Hou, Y., Tian, Y., Shen, C., Gao, H., & Liang, X. (2009). Solvothermal-assisted exfoliation process to produce graphene with high yield and high quality. *Nano Research*, 2(9), 706–712.
- [80] Le, L. T., Ervin, M. H., Qiu, H., Fuchs, B. E., & Lee, W. Y. (2011). Graphene supercapacitor electrodes fabricated by inkjet printing and thermal reduction of graphene oxide. *Electrochemistry Communications*, 13(4), 355–358.
- [81] Porro, S., & Ricciardi, C. (2015). Memristive behaviour in inkjet printed graphene oxide thin layers. *RSC Advances*, 5(84), 68565–68570.
- [82] Dua, V., Surwade, S. P., Ammu, S., Agnihotra, S. R., Jain, S., Roberts, K. E., ... Manohar, S. K. (2010). All-organic vapor sensor using inkjet-printed reduced graphene oxide. *Angewandte Chemie International Edition*, 49(12), 2154–2157.
- [83] Overgaard, M. H., Kühnel, M., Hvidsten, R., Petersen, S. V, Vosch, T., Nørgaard, K., & Laursen, B. W. (2017). Highly Conductive Semitransparent Graphene Circuits Screen-

Printed from Water-Based Graphene Oxide Ink. *Advanced Materials Technologies*, 2(7), 1700011.

- [84] Paton, K. R., Varrla, E., Backes, C., Smith, R. J., Khan, U., O'Neill, A., ... King, P. (2014). Scalable production of large quantities of defect-free few-layer graphene by shear exfoliation in liquids. *Nature Materials*, 13(6), 624–630
- [85] Lee, C.-L., Chen, C.-H., & Chen, C.-W. (2013). Graphene nanosheets as ink particles for inkjet printing on flexible board. *Chemical Engineering Journal*, 230, 296–302.
- [86] Chang, Q., Li, L., Sai, L., Shi, W., & Huang, L. (2018). Water-Soluble Hybrid Graphene Ink for Gravure-Printed Planar Supercapacitors. *Advanced Electronic Materials*, 4(8), 1800059.
- [87] Gao, Y., Shi, W., Wang, W., Leng, Y., & Zhao, Y. (2014). Inkjet printing patterns of highly conductive pristine graphene on flexible substrates. *Industrial & Engineering Chemistry Research*, 53(43), 16777–16784.
- [88] Xu, Y., Hennig, I., Freyberg, D., Strudwick, A. J., Schwab, M. G., Weitz, T., & Cha, K. C.-P. (2014). Inkjet-printed energy storage device using graphene/polyaniline inks. *Journal of Power Sources*, 248, 483–488.
- [89] Seekaew, Y., Lokavee, S., Phokharatkul, D., Wisitsoraat, A., Kerdcharoen, T., & Wongchoosuk, C. (2014). Low-cost and flexible printed graphene–PEDOT: PSS gas sensor for ammonia detection. *Organic Electronics*, 15(11), 2971–2981.
- [90] Pan, D., Gu, Y., Lan, H., Sun, Y., & Gao, H. (2015). Functional graphene-gold nanocomposite fabricated electrochemical biosensor for direct and rapid detection of bisphenol A. *Analytica Chimica Acta*, 853, 297–302.
- [91] Jabari, E., & Toyserkani, E. (2016). Aerosol-Jet printing of highly flexible and conductive graphene/silver patterns. *Materials Letters*, 174, 40–43.
- [92] Xu, L. Y., Yang, G. Y., Jing, H. Y., Wei, J., & Han, Y. D. (2014). Ag–graphene hybrid conductive ink for writing electronics. *Nanotechnology*, 25(5), 55201.
- [93] Liu, Z., Parvez, K., Li, R., Dong, R., Feng, X., & Müllen, K. (2015). Transparent conductive electrodes from graphene/PEDOT: PSS hybrid inks for ultrathin organic photodetectors. *Advanced Materials*, 27(4), 669–675.
- [94] Hyun, W. J., Park, O. O., & Chin, B. D. (2013). Foldable graphene electronic circuits based on paper substrates. *Advanced Materials*, 25(34), 4729–4734.
- [95] Wei, D., Andrew, P., Yang, H., Jiang, Y., Li, F., Shan, C., ... Bower, C. (2011). Flexible solid state lithium batteries based on graphene inks. *Journal of Materials Chemistry*, 21(26), 9762–9767

- [96] Casaluci, S., Gemmi, M., Pellegrini, V., Di Carlo, A., & Bonaccorso, F. (2016). Graphene-based large area dye-sensitized solar cell modules. *Nanoscale*, 8(9), 5368–5378.
- [97] Li, L., Secor, E. B., Chen, K., Zhu, J., Liu, X., Gao, T. Z., ... Hersam, M. C. (2016). High-Performance Solid-State Supercapacitors and Microsupercapacitors Derived from Printable Graphene Inks. *Advanced Energy Materials*, 6(20), 1600909.
- [98] Li, J., Sollami Delekta, S., Zhang, P., Yang, S., Lohe, M. R., Zhuang, X., ... Östling, M. (2017). Scalable fabrication and integration of graphene microsupercapacitors through full inkjet printing. *ACS Nano*, 11(8), 8249–8256.
- [99] Meng, H., Yang, W., Ding, K., Feng, L., & Guan, Y. (2015). Cu<sub>2</sub>O nanorods modified by reduced graphene oxide for NH<sub>3</sub> sensing at room temperature. *Journal of Materials Chemistry A*, 3(3), 1174–1181.
- [100] Ali, S., Hassan, A., Hassan, G., Bae, J., & Lee, C. H. (2016). All-printed humidity sensor based on graphene/methyl-red composite with high sensitivity. *Carbon*, 105, 23–32.
- [101] Kanso, H., García, M. B. G., Llano, L. F., Ma, S., Ludwig, R., Bolado, P. F., & Santos, D. H. (2017). Novel thin layer flow-cell screen-printed graphene electrode for enzymatic sensors. *Biosensors and Bioelectronics*, 93, 298–304.
- [102] Labroo, P., & Cui, Y. (2014). Graphene nano-ink biosensor arrays on a microfluidic paper for multiplexed detection of metabolites. *Analytica Chimica Acta*, 813, 90–96.
- [103] Deegan, R. D., Bakajin, O., Dupont, T. F., Huber, G., Nagel, S. R., & Witten, T. A. (1997). Capillary flow as the cause of ring stains from dried liquid drops. *Nature*, 389(6653), 827–829.
- [104] Jeong, S., Kim, D., & Moon, J. (2008). Ink-Jet-printed organic–inorganic hybrid dielectrics for organic thin-film transistors. *The Journal of Physical Chemistry C*, 112(14), 5245–5249.
- [105] Wang, S., Yi, M., & Shen, Z. (2016). The effect of surfactants and their concentration on the liquid exfoliation of graphene. *RSC Advances*, 6(61), 56705–56710.
- [106] Haiss, W., Thanh, N. T. K., Aveyard, J., & Fernig, D. G. (2007). Determination of size and concentration of gold nanoparticles from UV–Vis spectra. *Analytical Chemistry*, 79(11), 4215–4221.
- [107] Lotya, M., Hernandez, Y., King, P. J., Smith, R. J., Nicolosi, V., Karlsson, L. S., ... McGovern, I. T. (2009). Liquid phase production of graphene by exfoliation of graphite in surfactant/water solutions. *Journal of the American Chemical Society*, 131(10), 3611–3620.
- [108] Hernandez, Y., Nicolosi, V., Lotya, M., Blighe, F. M., Sun, Z., De, S., ... Gun'Ko, Y. K. (2008). High-yield production of graphene by liquid-phase exfoliation of graphite. *Nature Nanotechnology*, 3(9), 563.

- [109] Ager, D., Arjunan Vasantha, V., Crombez, R., & Texter, J. (2014). Aqueous graphene dispersions—optical properties and stimuli-responsive phase transfer. *ACS Nano*, 8(11), 11191–11205.
- [110] Yi, M., Shen, Z., Zhang, X., & Ma, S. (2012). Achieving concentrated graphene dispersions in water/acetone mixtures by the strategy of tailoring Hansen solubility parameters. *Journal of Physics D: Applied Physics*, 46(2), 25301.
- [111] Pecora, R. (2000). Dynamic light scattering measurement of nanometer particles in liquids. *Journal of Nanoparticle Research*, 2(2), 123–131.
- [112] Kaszuba, M., McKnight, D., Connah, M. T., McNeil-Watson, F. K., & Nobbmann, U. (2008). Measuring sub nanometre sizes using dynamic light scattering. *Journal of Nanoparticle Research*, 10(5), 823–829.
- [113] Jian, M., Wang, C., Wang, Q., Wang, H., Xia, K., Yin, Z., ... Zhang, Y. (2017). Advanced carbon materials for flexible and wearable sensors. *Science China Materials*, 60(11), 1026–1062.
- [114] Nepal, A., Singh, G. P., Flanders, B. N., & Sorensen, C. M. (2013). One-step synthesis of graphene via catalyst-free gas-phase hydrocarbon detonation. *Nanotechnology*, 24(24), 245602.
- [115] Popov, V. N. (2004). Carbon nanotubes: properties and application. *Materials Science and Engineering: R: Reports*, 43(3), 61–102.
- [116] Secor, E. B., Prabhumirashi, P. L., Puntambekar, K., Geier, M. L., & Hersam, M. C. (2013). Inkjet printing of high conductivity, flexible graphene patterns. *The Journal of Physical Chemistry Letters*, 4(8), 1347–1351.
- [117] Zhang, J., Wu, J., & Zhang, H. (2013). *PEM fuel cell testing and diagnosis*. Newnes.
- [118] Tang, L., Wang, Y., Li, Y., Feng, H., Lu, J., & Li, J. (2009). Preparation, structure, and electrochemical properties of reduced graphene sheet films. *Advanced Functional Materials*, 19(17), 2782–2789.
- [119] Luo, L., Zhu, L., & Wang, Z. (2012). Nonenzymatic amperometric determination of glucose by CuO nanocubes–graphene nanocomposite modified electrode. *Bioelectrochemistry*, 88, 156–163.
- [120] Wu, G., Song, X., Wu, Y.-F., Chen, X., Luo, F., & Chen, X. (2013). Non-enzymatic electrochemical glucose sensor based on platinum nanoflowers supported on graphene oxide. *Talanta*, 105, 379–385.